

SACLANTCEN MEMORANDUM
serial no.: SM-238

*SACLANT UNDERSEA
RESEARCH CENTRE*

MEMORANDUM



**Limitations on towed array gain
imposed by a non-isotropic ocean**

S. Stergiopoulos

August 1990

The SACLANT Undersea Research Centre provides the Supreme Allied Commander Atlantic (SACLANT) with scientific and technical assistance under the terms of its NATO charter, which entered into force on 1 February 1963. Without prejudice to this main task – and under the policy direction of SACLANT – the Centre also renders scientific and technical assistance to the individual NATO nations.

This document is released to a NATO Government at the direction of SACLAN T Undersea Research Centre subject to the following conditions:

- The recipient NATO Government agrees to use its best endeavours to ensure that the information herein disclosed, whether or not it bears a security classification, is not dealt with in any manner (a) contrary to the intent of the provisions of the Charter of the Centre, or (b) prejudicial to the rights of the owner thereof to obtain patent, copyright, or other like statutory protection therefor.
- If the technical information was originally released to the Centre by a NATO Government subject to restrictions clearly marked on this document the recipient NATO Government agrees to use its best endeavours to abide by the terms of the restrictions so imposed by the releasing Government.

Page count for SM-238
(excluding covers)

Pages	Total
i-iv	4
1-42	42
	<hr/>
	46

SACLANT Undersea Research Centre
Viale San Bartolomeo 400
19026 San Bartolomeo (SP), Italy

tel: 0187 540 111
fax: 0187 524 600
telex: 271148 SACENT I

NORTH ATLANTIC TREATY ORGANIZATION

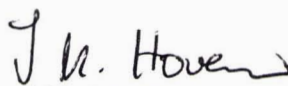
SACLANTCEN SM-238

Limitations on towed
array gain imposed by
a non-isotropic ocean

S. Stergiopoulos

The content of this document pertains
to work performed under Project 05 of
the SACLANTCEN Programme of Work.
The document has been approved for
release by The Director, SACLANTCEN.

Issued by:
Underwater Research Division


J.M. Hovem
Division Chief

**Limitations on towed array gain
imposed by a non-isotropic ocean**

S. Stergiopoulos

Abstract: This study deals with the limitations imposed by ocean characteristics on hydrophone array gain and on attempts to create a synthetic aperture using towed-array measurements. The multi-element synthetic or physical aperture of a passive array operates in a non-isotropic noise field and in a medium of limited spatial coherence length. In particular, it is assumed that due to distant shipping the noise field is partially directive and imposed upon an isotropic noise background, and in the rough bounded transmitted medium many multipaths exist which are closely spaced in arrival time and arrival angle. The coherence properties of the medium are synoptically considered to be characterized by its temporal coherence and the angular uncertainty which is the inverse of the spatial coherence length.

A processing scheme is suggested for the derivation of the array gain from received signals having small values of signal-to-noise ratio and for a given directivity pattern of the non-isotropic noise background. Simulations indicate that a comparison of predictions against experimental estimates for array gain can provide an approximate estimate of the coherence length of the medium. Real data applications, using the extended towed-array measurements technique, indicate that the physical aperture of an array can be extended successfully by more than one order of magnitude for cases of cw and broadband signals. This study concludes that the coherence properties of the ocean are sufficient for effective long towed-array applications and that a synthetic aperture can be created in an anisotropic medium.

Keywords: anisotropic medium ◦ array gain ◦ coherence ◦ conventional beamformer ◦ directivity power pattern ◦ extended towed-array measurements ◦ overlapped correlator ◦ synthetic aperture ◦ variance of estimates

Contents

1. Introduction	1
2. Theoretical remarks	3
2.1. <i>Spatial coherence</i>	4
2.2. <i>Coherence estimation</i>	6
2.3. <i>Array gain</i>	7
2.4. <i>Synthetic aperture</i>	8
3. Processing scheme for array gain estimates	11
4. Simulations	13
4.1. <i>Synthetic anisotropic noise</i>	13
4.2. <i>Real anisotropic ambient noise</i>	16
5. Experiments	22
5.1. <i>64-hydrophone towed array</i>	22
5.2. <i>256-hydrophone towed array</i>	27
6. Conclusions	39
References	41

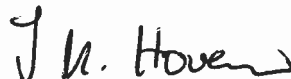
SACLANTCEN SM-238

Limitations on towed
array gain imposed by
a non-isotropic ocean

S. Stergiopoulos

The content of this document pertains
to work performed under Project 05 of
the SACLANTCEN Programme of Work.
The document has been approved for
release by The Director, SACLANTCEN.

Issued by:
Underwater Research Division


J.M. Hovem
Division Chief

1

Introduction

An acoustic signal that propagates through the ocean will interact with the transmitting medium microstructure and the rough boundaries, resulting in a scattered field that is characterized by irregular spatial and temporal variations. As a consequence of this interaction, a point source detected by a high-angular resolution receiver is perceived as a source of finite extent. It has been suggested by Wille and Thiele [1] that due to the above spatial variations the sound field consists not of parallel, but of superimposed wavefronts of different directions of propagation. As a result, coherence measurements of this field by a hydrophone array give an estimate for the spatial coherence function. In the model for the spatial uncertainty of the above study [1], the width of the coherence function is defined as the coherence length of the medium and its reciprocal value is a measure of the angular uncertainty caused by the scattered field of the underwater environment.

The mechanisms of scattering of acoustic signals from the sea surface [2–5], the bottom [6–9], the microstructures of the medium [10,11] and Arctic ice [12,13], which result in attenuation of the coherent component of sound, have been studied theoretically and experimentally for several decades. In spite of the effort that has been devoted to this field, there remain a number of diverse problems that would benefit from further study of scattering theory. Central to any scattering problem is a statistical model of the medium that determines the coherence of an acoustic signal in the sea. By the ‘coherence’ of acoustic signals in the sea we mean the degree to which the noise pressures are the same at two points in the sea located a given distance and direction apart. Pressure sensors (i.e. hydrophones) placed at these two points will have identical outputs if the received acoustic signals are perfectly coherent; if the two sensor outputs, as a function of space or time, are totally dissimilar, the signals are said to be incoherent. Thus, the loss of spatial coherence results in an upper limit on the useful aperture of a receiving array of hydrophones [14–18]. Consequently, the knowledge of the angular uncertainty of the signals caused by the medium is considered essential in order to define quantitatively the influence of the medium on the array gain, which is influenced significantly by a partially directive anisotropic noise background. Therefore, for a given non-isotropic underwater medium, it is desirable to estimate the optimum towed-array length and array gain for sonar and synthetic aperture applications.

The aim of the present investigation is to determine numerically the dependence of the array gain on the coherence length of the medium and on the directivity pattern of the noise field. In the theoretical discussion, a reasoned recommendation is

presented for signal processing to derive estimates of the array gain from received signals having small values of signal-to-noise ratio. Since the directivity pattern of the noise field is assumed to be known, a family of curves of the array gain ('array gain predictions for non-isotropic medium') is generated as a function of the array aperture and the coherence length of the medium. Experimental estimates of the array gain of a signal embodied in the above noise field are compared with the predicted array gain estimates, and an indication of the coherence length of the medium is derived. This is basically an approximate solution of the inverse problem for estimates of the coherence length of the ocean by using towed-array measurements. The physical processes defining the coherence properties of the medium are not examined in this study. However, models describing these properties have been considered here in order to estimate the array gain predictions for a non-isotropic underwater environment.

2

Theoretical remarks

Let us consider a line array in an anisotropic underwater medium. The array has N equally-spaced hydrophones with δ being their spacing and receives an acoustic signal from a distant source with bearing θ . The angle θ is measured from the broadside of the horizontal line array. The signal is sampled at time increment Δt with $t_i = i\Delta t$, where $i = 1, 2, \dots, M$, M being the number of data samples for each one of the hydrophone time series which are expressed by

$$x_n(t_i) = A \exp[-j2\pi f_0(t_i - (\delta(n-1)/c) \sin \theta)], \quad (1)$$

where $n = 1, 2, \dots, N$, A is the amplitude, and $X_n(f_0)$ is the fourier transform of $x_n(t_i)$ at the frequency f_0 .

Let $b(f_0, \theta)$ be the amplitude of the beam pattern of the array for the above signal. This amplitude is expressed by

$$b(f_0, \theta) = \sum_{n=1}^N \exp[-j2\pi f_0(t_i - (\delta(n-1) \sin \theta/c))] \quad (2)$$

and the power beam pattern $B(f_0, \theta)$ is given by $B(f_0, \theta) = b(f_0, \theta)b^\dagger(f_0, \theta)$, where the \dagger denotes complex conjugate. From Eq. (2) the power beam pattern $B(f_0, \theta)$ takes the form

$$B(f_0, \theta) = \sum_{n=1}^N \sum_{m=1}^N \exp[j2\pi f_0 \delta_{nm} \sin \theta/c], \quad (3)$$

where δ_{nm} is the spacing $\delta(n-m)$ between the n -th and m -th hydrophones. The correlation function in frequency domain for two hydrophone time series of the line array is given from $R_{nm}(f_0, \delta_{nm}) = X_n(f_0)X_m^\dagger(f_0)$. The above space frequency correlation function can be related to the angular power directivity pattern of the source, $\Psi_S(f_0, \theta)$, via a fourier transformation by using a generalization of Bello's concept [19] of time frequency correlation function [$t \leftrightarrow 2\pi f$] into space [$\delta_{nm} \leftrightarrow 2\pi f \sin \theta/c$], which gives

$$R_{nm}(f_0, \delta_{nm}) = \frac{1}{H_F} \int_{-\pi/2}^{\pi/2} \Psi_S(f_0, \theta) \exp[-j2\pi f_0 \delta_{nm} \theta/c] d\theta, \quad (4)$$

or

$$\Psi_S(f_0, \theta) = \frac{1}{H_I} \int_{-N\delta/2}^{N\delta/2} R_{nm}(f_0, \delta_{nm}) \exp[j2\pi f_0 \delta_{nm} \theta/c] d(\delta_{nm}), \quad (5)$$

where H_F, H_I are scaling constants. The above transformation is valid for small values of the angle θ (i.e. $\sin \theta \simeq \theta, \cos \theta \simeq 1$), which assumes that the source is at the broadside of the array. This assumption, however, is not required when the integral is converted into the following summation:

$$R_{nm}(f_0, \delta_{nm}) = \frac{\Delta\theta}{H_F} \sum_{g=-G/2}^{G/2} \Psi_S(f_0, \theta_g) \exp[-j2\pi f_0 \delta_{nm} \sin(g\Delta\theta)/c] \cos(g\Delta\theta),$$

where $\Delta\theta$ is the angle increment for sampling the angular power directivity pattern, $\theta_g = g\Delta\theta$, g is the index for the samples and G is the total number of samples.

The power directivity pattern of a distant source (calculated for a homogeneous free space) is supposed to be a delta function. Estimates, however, of the source's directivity from a line array operating in an anisotropic ocean are distorted by the underwater medium. In other words, at the input of the line array the directivity pattern of the received signal is the convolution of the original pattern and the angular directivity of the medium (i.e. the angular scattering function of the underwater environment). As a result of the above, if the original angular directivity pattern of the source is a delta beam, then the angular pattern of the received signal is the scattering function of the medium.

2.1. SPATIAL COHERENCE

In ocean acoustics the wave propagation problem is characterized by a high complexity due to the spatial properties of the nonhomogeneous underwater environment. The space time properties of the ocean acoustic pressure field, for stationary source and receivers, include a limiting resolution imposed by the medium for a line array of hydrophones. This limitation is due either to the angular spread of the incident energy about a single arrival as a result of the scattering phenomena, or to the multipaths and their variation over the aperture of the hydrophone array. A thorough discussion of the relative importance of these effects on the underwater acoustics measurement problem has been given by Carey and Moseley [26]. Investigation of these effects, however, is beyond the scope of this paper, and we refer the reader to some excellent reviews [27,28].

In this study, the term spatial coherence means the statistical response of a line array to the acoustic field. This response is the result of the multipath and scattering phenomena discussed before, and there are models [1,25,29] to relate the spatial coherence with the physical parameters of the underwater medium for measurements interpretation. In these models, the interaction of the acoustic signal with the transmitting medium is considered to result in superimposed wavefronts of different directions of propagation. Then the received signal by the n -th hydrophone of an

array is expressed by

$$x_n(t_i) = \sum_{l=1}^K A_l \exp[-j2\pi f_l(t_i - \delta(n-1)\theta_l/c)], \quad (6)$$

where $l = 1, 2, \dots, K$, and K is the number of superimposed waves; a generalized form of the crosscorrelation function between two sensors, which has been discussed by Carey and Moseley [26], is

$$R_{nm}(f_0, \delta_{nm}) \simeq \bar{X}^2(f_0) \exp[-(\delta_{nm}/L_0)^k], \quad k = 1, 1.5, 2 \quad (7)$$

where L_0 is the correlation length and $\bar{X}^2(f_0)$ is the mean acoustic intensity of a hydrophone time sequence of the array. The exponential form of the above expression for $k = 1.5$ has been suggested by Beran and McCoy [29], and the one for $k = 2$, which is the gaussian form, has been proposed by Wille and Thiele [1]. A review of these models is given elsewhere [26]. It is assumed in the present study that the acoustic field is gaussian and this is translated here as a gaussian distribution of the directions of propagation with mean directional standard deviation σ_θ , called 'angular uncertainty of the medium', for the superimposed waves received by the sensors of the line array. A more explicit expression for the gaussian form of the Eq. (7) is [1]

$$R_{nm}(f_0, \delta_{nm}) \simeq \bar{X}^2(f_0) \exp[-\frac{1}{2}(2\pi f_0 \delta_{nm} \sigma_\theta / c)^2], \quad (8)$$

and the cross-correlation coefficients are given from $\rho_{nm}(f_0, \delta_{nm}) = R_{nm}(f_0, \delta_{nm}) / \bar{X}^2(f_0)$. At the distance $L_c = c/(2\pi f_0 \sigma_\theta)$, called 'coherence length', the correlation function in Eq. (8) will be 0.6. This critical length is determined from experimental coherence measurements plotted as a function of δ_{nm} . Then a connection between the medium angular uncertainty and the measured coherence length is derived as

$$\sigma_\theta = 1/L_c, \quad \text{and} \quad L_c = 2\pi \delta_{1m} f_0 / c, \quad (9)$$

where δ_{1m} is the critical distance between the first and the m -th sensors at which the coherence measurements get smaller than 0.6. The above parameter definition will be used in this study to interpret experimental measurements of the angular uncertainty of the medium that influences the performance of a line array.

Since the correlation function for a gaussian acoustic field is given from Eq. (8), the angular scattering function $\Phi(f_0, \theta)$ of the medium can be derived. Using Eq. (5) and following a rather simple analytical integral evaluation, we have

$$\Phi(f_0, \theta) = \frac{1}{\sigma_\theta \sqrt{2\pi}} \exp[-\theta^2 / 2\sigma_\theta^2], \quad (10)$$

where $\sigma_\theta = c/2\pi f_0 \delta_{nm}$. This expression for the angular scattering function of a gaussian acoustic field has been proposed by Wille and Thiele [1].

2.2. COHERENCE ESTIMATION

It is apparent from the above discussion that the estimates of the crosscorrelation coefficients $\rho_{nm}(f_0, \delta_{nm})$ are necessary in order to define experimentally the coherence length of an underwater medium. Therefore, it is considered appropriate here to discuss briefly the coherence estimation problem.

It is well known that a stationary homogeneous gaussian acoustic field is completely characterized by its space-time correlation function. When there is a large number of propagation paths of acoustic signals and the fluctuations of the path parameters are such that the received signals satisfy a central limit theorem, then the sound field received by a line array of hydrophones is gaussian. The degree of coherence of the acoustic field is expressed quantitatively by the same coefficient that is used in statistics to express the degree of dependence between two variables, and it is a normalized cross spectral density function.

In the present study, it is assumed that the acoustic field is gaussian or that the acoustic signals received by two hydrophones located at a given distance and direction apart are two random processes $x_n(t)$ and $x_m(t)$ with auto spectra $X_n^2(f)$ and $X_m^2(f)$, respectively, and cross spectrum $R_{nm}(f, \delta_{nm})$. The coherence between these two signals is defined as

$$\gamma_{nm}(f) = \frac{|R_{nm}(f, \delta_{nm})|}{|X_n(f)||X_m(f)|}. \quad (11)$$

Estimates of $\gamma_{nm}(f)$ are available [22] and are provided from K segments of the $x_n(t)$ and $x_m(t)$ time series according to

$$\tilde{\gamma}_{nm}(f, \delta_{nm}) = \frac{|\sum_{l=1}^K X_{n_l}(f)X_{m_l}^\dagger(f)|}{\sqrt{\sum_{l=1}^K |X_{n_l}(f)|^2 \sum_{i=1}^K |X_{m_i}(f)|^2}}, \quad (12)$$

where $X_{n_l}(f)$ and $X_{m_l}(f)$ are the fourier coefficients at frequency f , obtained from the l -th weighted segments and \dagger denotes complex conjugate. There has been much related work on statistics and the probability density function and derivations of a maximum likelihood estimator of $\tilde{\gamma}(f)$ [22,23]. The conclusion from these studies is an estimate of the m th moments of $\tilde{\gamma}(f)$ when the coherence estimates are derived from Eq. (12) for K degrees of freedom.

When large numbers of segments are needed to be obtained from time series including acoustic signals from explosives, then there are practical limitations in using Eq. (12) as a coherence estimator. This is because the above time series could provide only a very small number of segments. To avoid the above limitation, an assumption is made that within a limited frequency band the condition of stationarity in frequency might be valid. This of course is not valid over the whole frequency range; otherwise,

it could not be expected any frequency dependence of the coherence function and would have only a coherence coefficient. For a sufficient narrow frequency band with central frequency f_0 and observation bandwidth Δf or $f_0 - \frac{1}{2}\Delta f \leq f_0 \leq f_0 + \frac{1}{2}\Delta f$ we have a coherence estimate according to

$$\tilde{\gamma}_{nm}(f_0, \delta_{nm}) = \frac{|\sum_{l=1}^Q X_n(f_l) X_m^\dagger(f_l)|}{\sqrt{\sum_{l=1}^Q |X_n(f_l)|^2 \sum_{l=1}^Q |X_m(f_l)|^2}}, \quad (13)$$

where $f_l, l = 1, 2, \dots, Q$ are the frequency bins in the band $f_0 - \frac{1}{2}\Delta f \leq f_0 \leq f_0 + \frac{1}{2}\Delta f$ with central frequency f_0 . The above coherence estimators in Eqs. (12) and (13) are equivalent since they exploit the dispersive nature of the medium in the time and frequency domains. In particular, the time dispersion is observed when an impulse response is received at long range as a series of peaks in the acoustic time series. This time dispersion is equivalent in frequency domain to a frequency dispersion that is observed when a very stable cw sound source is received as a narrow band, but not zero bandwidth, process.

2.3. ARRAY GAIN

The performance of a line array to an acoustic signal embodied in a partially directive noise field is characterized by the ‘array gain’, which is defined by [30]

$$G = 10 \log \frac{\int \Psi_S(\theta, \phi) B(\theta, \phi) d\Omega / \int \Psi_S(\theta, \phi) d\Omega}{\int \Psi_N(\theta, \phi) B(\theta, \phi) d\Omega / \int \Psi_N(\theta, \phi) d\Omega}, \quad (14)$$

where $\Psi_S(\theta, \phi), \Psi_N(\theta, \phi)$ are the signal and noise power per unit solid angle $d\Omega$, respectively, and $B(\theta, \phi)$ is the power beam pattern of the line array. It is assumed here that the directivity power patterns $\Psi_S(\theta, \phi), \Psi_N(\theta, \phi), B(\theta, \phi)$ have rotational symmetry about the axis of the horizontal line array. Then Eq. (14) is modified to

$$G = 10 \log \frac{\int [\Psi_S(\theta) B(\theta) \cos \theta] d\theta / \int [\Psi_S(\theta) \cos \theta] d\theta}{\int [\Psi_N(\theta) B(\theta) \cos \theta] d\theta / \int [\Psi_N(\theta) \cos \theta] d\theta}. \quad (15)$$

The integrals $\int [\Psi_S(f_0, \theta) \cos \theta] d\theta, \int [\Psi_N(f_0, \theta) \cos \theta] d\theta$ are equal to $\tilde{X}_S^2(f_0), \tilde{X}_N^2(f_0)$ for the signal and the noise respectively, as follows from Eqs. (5), (8) and (10). Since the power beam pattern $B(\theta)$ of the line array is expressed by Eq. (3) and it has been assumed in this study that the original directivity pattern of the source is a delta beam, the relation (15) is modified to

$$G = 10 \log \frac{\sum_{n=1}^N \sum_{m=1}^N \sum_{g=-G/2}^{G/2} [\Phi(f_0, \theta_g) \exp[-j2\pi f_0 \delta_{mn} \sin(g\Delta\theta)/c] \cos(g\Delta\theta)]}{\sum_{n=1}^N \sum_{m=1}^N \sum_{g=-G/2}^{G/2} [\Psi_N(f_0, \theta_g) \exp[-j2\pi f_0 \delta_{mn} \sin(g\Delta\theta)/c] \cos(g\Delta\theta)]} - 10 \log(\tilde{X}_S^2(f_0)/\tilde{X}_N^2(f_0)), \quad (16)$$

where the directivity pattern of the received signal $\Psi(f_0, \theta)$ has been replaced by the angular scattering function $\Phi(f_0, \theta)$ of the medium. By using the summation form of Eq. (4), the expression (16) is simplified into the following form:

$$G = 10 \log \frac{\sum_{n=1}^N \sum_{m=1}^N \rho_{S_{nm}}(f_0, \delta_{nm})}{\sum_{n=1}^N \sum_{m=1}^N \rho_{N_{nm}}(f_0, \delta_{nm})} \quad (17)$$

and $\rho_{S_{nm}}(f_0, \delta_{nm}) = R_{nm}(f_0, \delta_{nm})/\tilde{X}_S^2(f_0)$. Equation (17) is the well-known expression for the array gain.

It is important to note here that in expression (16) the array gain includes the spatial characteristics of the medium together with the power directivity pattern of the noise field. This expression will be used later to derive predictions for the spatial coherence length of a medium by assuming that the angular directivity pattern of the acoustic noise field is known.

2.4. SYNTHETIC APERTURE

The results of the above theoretical discussion are related to the physical aperture of line arrays. Therefore, questions can be raised about the use of the above results to synthetic aperture applications. This subsection deals with these questions based on results from numerical and successful experimental applications of passive synthetic aperture processing techniques.

It has been shown [21,25] that the problem of creating a passive synthetic aperture is centered on the estimation of a phase correction factor, which is used to compensate for the phase between different in time towed-array measurements in order to synthesize coherently their space information into a synthetic aperture. When the estimates of this phase correction factor are correct, then the information inherent in the synthetic aperture is the same as that of an equivalent in size physical aperture. This equivalence has been investigated and for more information the reader is referred to other studies [24,25]. Therefore, the discussion in the previous sections should also be applicable to synthetic aperture applications.

The phase correction estimates, however, for synthetic aperture applications require knowledge of the speed V of the towed array and accurate estimates for the frequency

of the received signal. An additional restriction is that the synthetic aperture processing techniques have to compensate also for the disturbed paths of the towed array, which influence the synthetic aperture process very badly.

Recently, only two passive synthetic aperture techniques and one MLE estimator [21,24,25] have been published in the open literature that deal successfully with the above restrictions. Their real data application results have indicated that the formation of a synthetic aperture in the sea is feasible when the spatial coherence length of the medium is at least equal to the synthetic aperture length. It has been also shown that in one of the above synthetic aperture schemes (i.e. ETAM algorithm [21]), the phase correction estimates will introduce an increase in the variance of the phase term, which includes the directional information of the source. This increase in the phase variance follows a random-walk iterative procedure, which must break down at some maximum value of a synthetic aperture length. More explicitly, if the aperture of a N -hydrophone towed array is extended to a synthetic aperture with qN hydrophones, the ETAM algorithm requires $2(q-1)$ iterations to synthesize this qN -element array. During the μ th iteration, the phase variance increases by $\sigma_{\psi\mu}^2 = \sigma_{\psi}^2(2\mu/N)$, where σ_{ψ}^2 is the phase variance of one hydrophone phase term of the N -element physical array during the first iteration. At the end of the synthesizing procedure, which is the $2(q-1)$ th iteration, the phase variance will be $\sigma_{\psi^{2(q-1)}}^2 = \sigma_{\psi}^2(4(q-1)/N)$.

Let us consider, for example, the case of a medium with 128λ spatial coherence length and a towed array with a physical aperture equal to 16λ , where λ is the wavelength of the received acoustic signal. In this case, applications of the ETAM algorithm to extend the physical aperture of the array to 128λ require 14 iterations. Then the phase variance σ_{ψ}^2 at the 14th iteration will be $\sigma_{\psi^{14}}^2 \simeq \sigma_{\psi}^2$, which is not a dramatic increase. It is important to note here that in this example the increase during each iteration of the phase variance will be linearly distributed along the synthetic aperture. In other words, each 8λ subaperture of the 128λ synthetic array will have a phase variance increase by $0.06\sigma_{\psi}^2$. This example suggests that the breakdown of a synthetic aperture procedure will be caused by the limited spatial coherence length of the medium and not by the random-walk iterative procedure of the ETAM algorithm, since the value of 128λ is considered as an upper limit for the spatial coherence length of the medium.

The above discussion leads to a conclusion that a synthetic aperture scheme will induce an increase in the variance of the phase terms, which include the directional information of the source along the hydrophones of the synthetic array. This is equivalent to a decrease in the values of the coherence coefficients between hydrophones of the synthetic array and this decrease results in a reduction of the array gain. The determination of a line array's response to hydrophone time series with a given phase variance has been thoroughly discussed by Shifrin [31]. His results include an analytical evaluation of the angular power pattern of a line array as a function of the phase variance and the size of the correlation length, which in our case is

the spatial coherence length L_c of the medium. Thus, the results of the theoretical discussion in the previous sections can be used in synthetic aperture applications. In the present study, the ETAM algorithm has been selected for synthetic aperture application (reported in Sect. 5) because the performance and the increase in the phase variance induced by this algorithm are known.

Processing scheme for array gain estimates

In what follows an attempt is made to develop a signal processing scheme for array gain estimates from towed-array measurements that do not have high values of signal-to-noise ratio.

Let us consider $A_0 x_{S_n}(t)$ to be the signal of a distant source, $W_0 x_{N_n}(t)$ to be the partially directive noise signal due to distant shipping traffic and environmental effects, and $x_n(t)$ to be the received signal by the n th hydrophone of the line array expressed by

$$x_n(t) = A_0 x_{S_n}(t) + W_0 x_{N_n}(t), \quad (18)$$

where A_0, W_0 are the amplitude for the signal and the non-isotropic noise. The correlation function for the signals received at the n th and m th hydrophone is

$$r_{nm}(\tau) = \frac{1}{N} \sum_{k=1}^{N-l} [A_0^\dagger x_{S_n}^\dagger(t_k) + W_0^\dagger x_{N_n}^\dagger(t_k)] [A_0 x_{S_m}(t_{k+l}) + W_0 x_{N_m}(t_{k+l})], \quad (19)$$

or

$$r_{nm}(\tau) = A_0^2 r_{S_{nm}}(\tau) + W_0^2 r_{N_{nm}}(\tau) + \frac{1}{N} \sum_{k=1}^{N-l} [A_0^\dagger W_0 x_{S_n}^\dagger(t_k) x_{N_m}(t_{k+l}) + W_0^\dagger A_0 x_{N_n}^\dagger(t_k) x_{S_m}(t_{k+l})], \quad (20)$$

and $\tau = l\Delta t$, $r_{S_{nm}}(\tau)$, $r_{N_{nm}}(\tau)$ are the normalized correlation functions for the signal and noise, respectively. It is assumed here that the signal $x_{S_n}(t)$ and the noise $x_{N_n}(t)$ are uncorrelated; the validity of this assumption will be tested later with real data applications. Then the summation term in the right-hand side of Eq. (20) vanishes, and the correlation function $r_{nm}(\tau)$ in frequency domain is expressed by

$$R_{nm}(f_0, \delta_{nm}) = \tilde{X}_S^2(f_0) \rho_{S_{nm}}(f_0, \delta_{nm}) + \tilde{X}_N^2(f_0) \rho_{N_{nm}}(f_0, \delta_{nm}) \quad (21)$$

where $\rho_{S_{nm}}(f_0, \delta_{nm})$, $\rho_{N_{nm}}(f_0, \delta_{nm})$ are the normalized correlation functions in frequency domain for the signal and the noise, respectively. The parameters $\tilde{X}_S^2(f_0)$, $\tilde{X}_N^2(f_0)$ are the mean acoustic intensities at the frequency f_0 for the signal and the noise. The signal-to-noise ratio is defined as $\varsigma = 10 \log(\tilde{X}_S^2(f_0)/\tilde{X}_N^2(f_0))$. From Eq. (21) and using expression (5), the angular directivity pattern of the received signal $\Psi(f_0, \theta)$ can be derived, which is

$$\Psi(f_0, \theta) = \Psi_S(f_0, \theta) + \Psi_N(f_0, \theta), \quad (22)$$

and $\Psi_S(f_0, \theta)$, $\Psi_N(f_0, \theta)$ are the angular directivity patterns of the signal and the noise. As expected, the results in Eq. (22) show that the power directivity pattern of the received signal is the superposition of the patterns of the signal and the noise. Equation (22) is valid under the assumption that the characteristics of the source are not correlated with the partially directive acoustic noise field due to distant shipping.

In most of the cases, the characteristics of the ambient noise (i.e. $\tilde{X}_N^2(f_0)$, $\Psi_N(f_0, \theta)$) due to distant shipping and other environmental noise sources are known or they can be estimated for a specific area by statistical means from long time observations. In Eq. (22), the angular power pattern $\Psi(f_0, \theta)$ of the received signal is estimated directly from the towed-array measurements. The signal-to-noise ratio ς and the parameters $\tilde{X}_N^2(f_0)$, $\Psi_N(f_0, \theta)$ of the noise field have been assumed to be known. Then, estimates of $\Psi_S(f_0, \theta)$ can be derived from Eq. (22) and the array gain is calculated according to Eq. (17) from the correlation coefficients $\rho_{S_{nm}}(f_0, \delta_{nm})$, $\rho_{S_{nm}}(f_0, \delta_{nm})$, which are estimated numerically using the known quantities ς , $\tilde{X}_N^2(f_0)$, $\Psi_N(f_0, \theta)$, $\Psi_S(f_0, \theta)$ and Eq. (4) in summation form.

It is important to note here that in the above array gain processing scheme the smallest value of signal-to-noise ratio ς needs to be higher than 5 dB in the frequency bin, which is the value that will provide a clear distinction between the $\Psi(f_0, \theta)$ and $\Psi_N(f_0, \theta)$ power patterns in order to get estimates of $\Psi_S(f_0, \theta)$. The above threshold value of this processing scheme has been established empirically from simulations.

Further, predictions of the array gain for a specific area with known acoustic noise characteristics (i.e. $\tilde{X}_N^2(f_0)$, $\Psi_N(f_0, \theta)$) and for different values of spatial coherence length of the medium can be derived from Eq. (16). This is of practical importance, since a comparison of array gain measurements from towed-array data for an area where the above kind of predictions are available would lead to approximate estimates of the coherence length of the underwater medium of this area. The above approach will be tested in Sect. 4 with numerical simulation examples.

4.1. SYNTHETIC ANISOTROPIC NOISE

Cron and Sherman [32] introduced a model for surface noise generation, described by $\cos^\nu \theta$, which is the pressure directionality function and $\nu \geq 1$ is a measure of the anisotropy of the noise field. For this angular directionality of the noise field, the normalized correlation function $\rho_{nm}(f_0, \delta_{nm})$ can be expressed as

$$\rho_{nm}(f_0, \delta_{nm}) = 2^\nu \nu! J_\nu((2\pi f_0/c)\delta_{nm}) / ((2\pi f_0/c)\delta_{nm})^\nu, \quad \nu \geq 1. \quad (23)$$

The directionality pattern that is derived from Eq. (23) refers to the nearfield noise that is received from a vertical line array. In order to test with simulations, however, the theoretical development and the processing scheme for array gain estimates, that have been discussed in Sect. 3, it has been chosen in this study to use the above noise model as a farfield anisotropic noise, since the related correlation coefficients for the directionality pattern are known from Eq. (23).

Shown in Fig. 1 are towed-array gain predictions as a function of the array aperture size, for different values of spatial coherence length of the medium (i.e. $L_c = (512, 100, 32, 16, 8)\lambda$) and for cases of isotropic and non-isotropic noise. For the case of isotropic noise, the denominator in Eq. (17) is equal to $\sum_{n=1}^N \sum_{m=1}^N \rho_{N_{nm}}(f_0, \delta_{nm}) = N$, since the noise correlation coefficients for $n \neq m$ are negligible. The synthetic non-isotropic noise was generated from the Cron and Sherman model for $\nu = 3$ and its correlation coefficients were given from Eq. (23). Estimates of the correlation coefficients $\rho_{S_{nm}}(f_0, \delta_{nm})$ of the signal were given from expression (8), which is a function of the coherence length of a medium. Then, the array gain predictions can be derived from Eq. (16) or (17).

A 64-hydrophone towed-array response for the above synthetic anisotropic noise field (i.e. $\nu = 3$) is shown in Fig. 2a. In the same figure, the beam pattern of a source signal propagating in a medium with 512λ spatial coherence length is presented by the dashed line. The towed-array response for the received signal that includes the noise and the above source signal is given by the solid line of this figure. The signal-to-noise ratio in this case was $\varsigma = 10$ dB in the frequency bin. The frequency of the signal was 400 Hz and the spacing between the hydrophones in the array was $\frac{1}{2}\lambda$. Figure 2b has the same information as Fig. 2a but for a medium with 8λ coherence length.

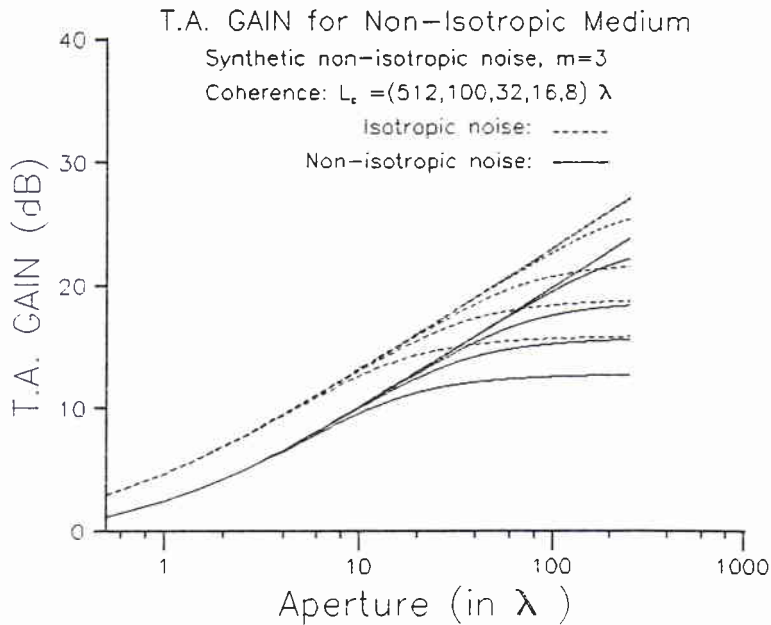


Figure 1 Line array gain predictions as a function of the array aperture size and for different values of spatial coherence length of the medium (i.e. $L_c = (512, 100, 32, 16, 8)\lambda$). Shown by the dashed lines are array gain predictions for isotropic noise field. The solid lines give array gain predictions for synthetic non-isotropic noise, which was generated from the Cron and Sherman model for $\nu = 3$.

Since the correlation coefficients for the noise and the signal in Figs. 2a and 2b are known, the expected values of the towed-array gain can be estimated directly from Eq. (17). These expected values, which agree with the predictions from Eq. (16), are shown in Figs. 2a and 2b. Array gain estimates for the set of data in Figs. 2a and 2b have also been calculated using the processing scheme that was introduced in Sect. 3, and the results are presented in Fig. 3 together with the array gain predictions for the above anisotropic noise field and for different values of the medium coherence length. Gain estimates for a 128-hydrophone towed array have been derived in the same way and their values are also plotted in Fig. 3. The data points indicated by a star symbol in this figure correspond to 64-hydrophone and 128-hydrophone array gain estimates and for 8λ coherence length of the medium. For the same arrays and measurement arrangement as before, the data points shown by an hexagon correspond to 512λ coherence length. Clearly, these array gain estimates are slightly smaller by 1.2 dB from their predicted values, and this difference is due to the effects of the array gain processing scheme and the rather small value of the signal-to-noise ratio of the above simulated signal. Other sets of simulations, however, have shown that for very high values of signal-to-noise ratio (i.e. $\zeta \geq 20$ dB) there is a good agreement between the estimated and the predicted array gain estimates.

SACLANTCEN SM-238

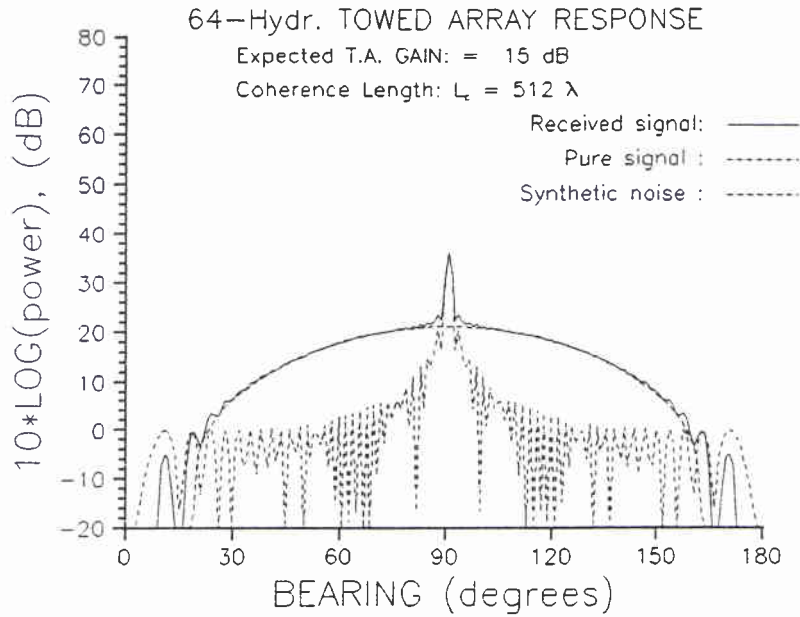


Figure 2a A 32λ array response for (1) a source signal propagating in a medium with 512λ spatial coherence length, which is shown by the dotted line; (2) the synthetic non-isotropic noise field generated from the Cron and Sherman model for $\nu = 3$, which is shown by the dashed line; and (3) the received signal including the source signal and the non-isotropic noise, is shown by the solid line. The source signal and the anisotropic noise have been scaled according to the desired value of signal-to-noise ratio, which for this case is $\zeta = 10$ dB in the frequency bin. The expected array gain for the source signal is 15 dB.

A comparison in Fig. 3 between the estimated array gains using the above processing scheme and the array gain predictions from Eq. (16) indicates that the above inversion method provides approximate estimates of the coherence length of the medium. In fact, a single array gain estimate from towed-array measurements related to a medium with the noise characteristics known, is sufficient to provide an indication of the coherence length of this medium.

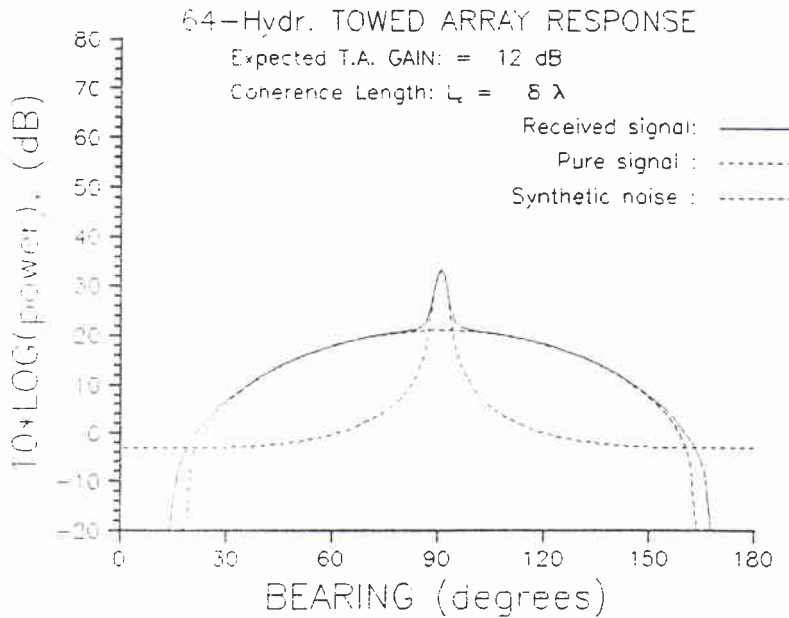


Figure 2b A 32λ line array response for a source signal propagating in a medium with 8λ spatial coherence length. The results of this figure have been arranged in the same way as in Fig. 2a. The expected array gain for the above source signal is 12 dB.

4.2. REAL ANISOTROPIC AMBIENT NOISE

Figure 4 gives the horizontal directionality of the acoustic noise field due to distant shipping for a specific area in the Mediterranean Sea. The arrow at 30° bearing shows the broadside direction of a 64-hydrophone towed array, which is considered for the following set of simulations. This directionality pattern is for 50 Hz frequency and was derived using a technique developed by Wagstaff [33]. For the above noise angular pattern the correlation coefficients of the anisotropic noise field for the 64-hydrophone towed array have been derived using Eq. (4) in summation form. In one set of simulations, the correlation coefficients of a synthetic signal propagating in a medium with 512λ coherence length were generated by using Eq. (8). The correlation coefficients of this signal were added to those of the anisotropic noise following a scaling according to the value of signal-to-noise ratio, which was considered to be $\zeta = 10$ dB in the frequency bin. This operation provided the correlation coefficients of a received signal including real anisotropic noise and synthetic source signal for a medium with known spatial coherence length.

Figure 5 shows the response of a 64-hydrophone towed array with $\frac{1}{2}\lambda$ spacing for the above received signal, the real anisotropic noise and the synthetic signal for a medium with 512λ coherence length. The expected array gain is 11 dB and it has been estimated from Eq. (17) since the correlation coefficients for the signal and the noise are known from the above simulation procedure. Another estimate also of the array gain has been derived by applying the array gain processing scheme on

 SAACLANTCEN SM-238

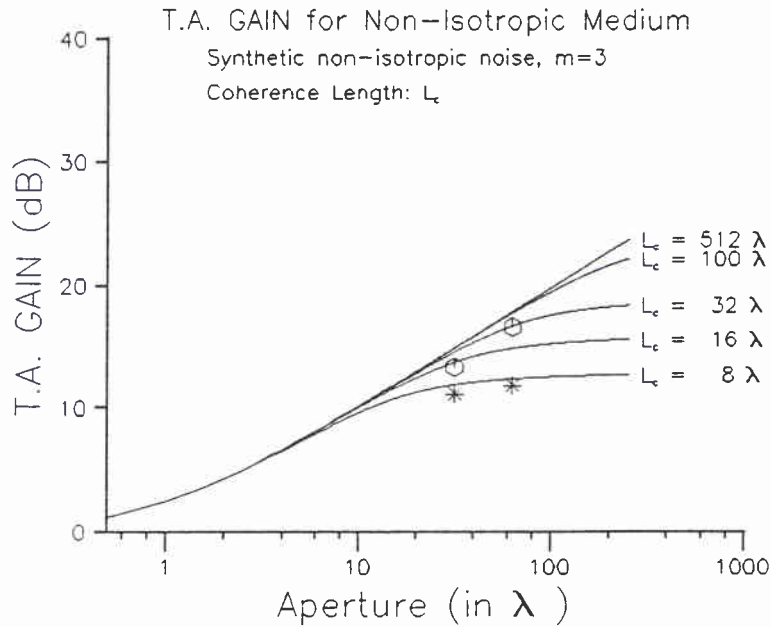


Figure 3 Shown by the solid lines are the array gain estimates for synthetic anisotropic noise field and for different values of spatial coherence length of the medium (i.e. $L_c = (512, 100, 32, 16, 8)\lambda$). These predictions are the same with those of Fig. 1. The data points indicated by a star symbol correspond to array gain estimates for a source signal propagating in a medium with 8λ coherence length and for 32λ and 64λ line arrays. Shown by the hexagon-shaped data points are array gain estimates for a signal propagating in a 512λ coherence length medium and for 32λ and 64λ line arrays. The processing scheme that has been used to derive these array gain estimates has been discussed in Sect. 3.

the received signal and the ambient-noise directionality patterns. This new estimate is 9.9 dB and it is smaller than its expected value since the signal-to-noise ratio is rather small.

For the above ambient-noise directivity pattern, the array gain predictions are derived in the same way as in Subsect. 4.1 and are shown in Fig. 6 by the solid lines. These lines are for different values of spatial coherence length of the medium (i.e. $L_c = 512, 32, 16, 8\lambda$). The dashed lines in the Fig. 6 present the array gain predictions for isotropic noise and for the same values of coherence length as before. The data points indicated by a star symbol correspond to array gain estimates using the above processing scheme for a received signal in a medium with 512λ and 8λ coherence length. However, the consideration in this section about the acoustic field due to distant shipping to be taken as anisotropic noise is arbitrary, and for others this noise field can be treated as signal. Then, for the above set of simulated received signals and for the case of an isotropic noise field, the new values of the array gains are estimated in the same way as before, assuming that the correlation coefficients

HORIZONTAL DIRECTIONALITY

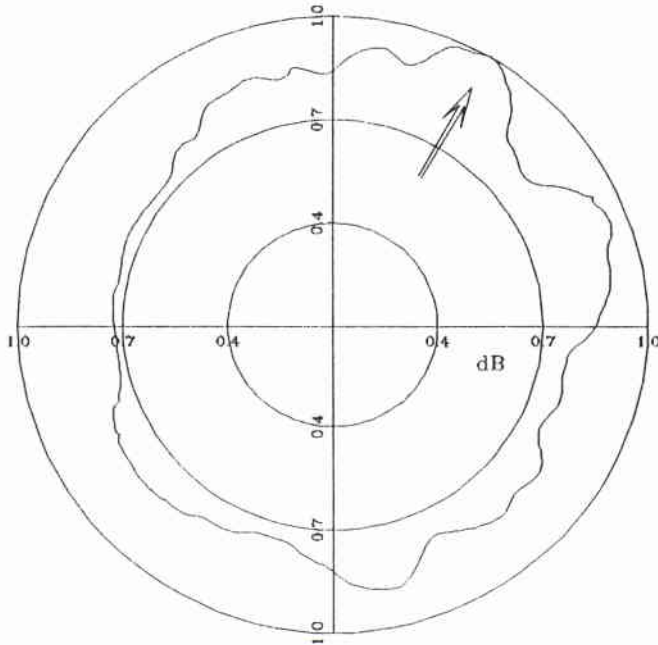


Figure 4 Horizontal directionality pattern of the acoustic noise field at 50 Hz due to distant shipping for a specific area in the Mediterranean sea. The arrow at 30° bearing shows the broadside direction of a 64-hydrophone towed array, which is considered for simulations.

of the noise are $\sum_{n=1}^N \sum_{m=1}^N \rho_{N_{nm}}(f_0, \delta_{nm}) = N$. These new estimates are indicated by the hexagon-shaped data point, which have been plotted in Fig. 6.

If the broadside direction of the towed array is considered to be at 270° bearing in the anisotropic noise field that is shown in Fig. 5, then the estimates of the array gain should improve because the noise field is not as directive as in the case of 30° bearing that was examined before. The above expectation is correct and it is demonstrated by the improved array gain estimates and predictions, shown in Fig. 7, of another set of simulations that included a broadside direction for the line array at 270° bearing.

A comparison between the results of Figs. 6 and 7 indicates that in the case of an isotropic noise field the array gain predictions and estimates are identical even though they come from different set of simulated signals. On the other hand, the results for the case of the anisotropic noise field demonstrate that the array gain estimates and predictions are improved when the broadside direction of the towed array is at a bearing with the minimum noise directivity. It is also equally important to note here that a comparison in Figs. 6 and 7 between the array gain predictions and estimates provides an approximate estimate of the simulated medium coherence length.

SACLANTCEN SM-238

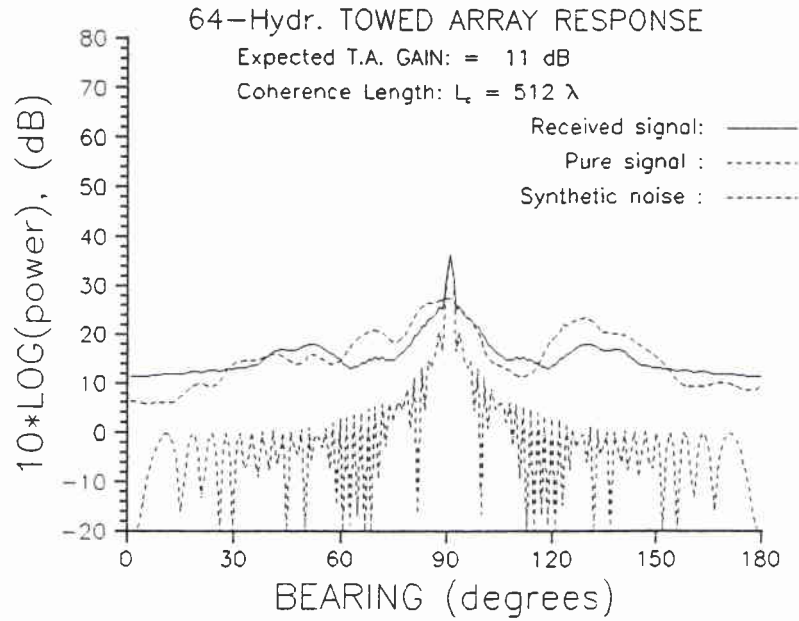


Figure 5 A 32λ array response for (1) a synthetic source signal propagating in a medium with 512λ spatial coherence length which is shown by the dotted line; (2) a real non-isotropic noise field, the same as in Fig. 4, which is shown by the dashed line; and (3) the received signal including the source signal and the non-isotropic noise is shown by the solid line. The source signal and the anisotropic noise have been scaled according to the desired value of signal-to-noise ratio, which for this case is $\zeta = 10$ dB in the frequency bin. The expected array gain for the above source signal is 11 dB.

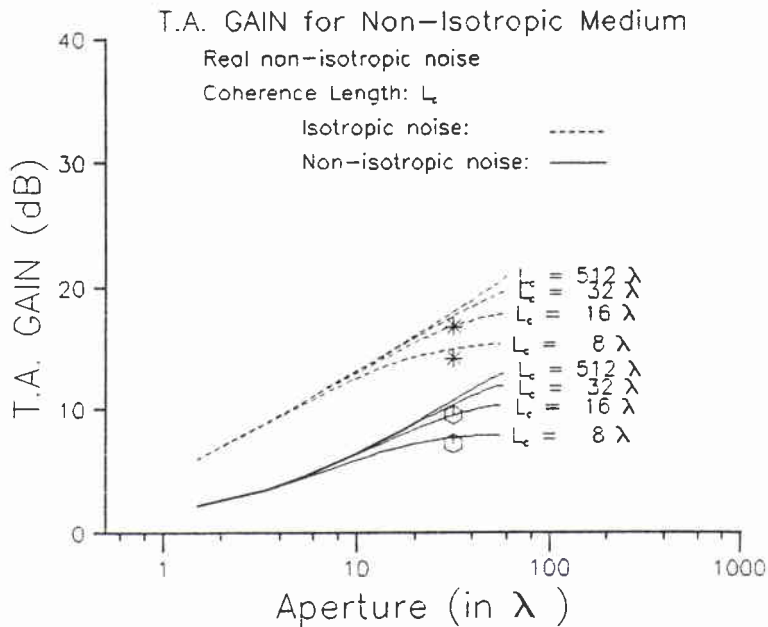


Figure 6 Shown by the solid lines are the array gain estimates for the anisotropic noise field of Fig. 4, for different values of spatial coherence length of the medium (i.e. $L_c = (512, 32, 16, 8)\lambda$). The dashed lines give the array gain predictions for isotropic noise field and for the same values of spatial coherence length as before. The data points indicated by a star symbol correspond to array gain estimates for isotropic noise field, for a source signal propagating in a medium with 8λ , 512λ coherence length, and for a 32λ line array. Shown by the hexagon-shaped data points are array gain estimates for the real anisotropic noise field of Fig. 4, for a signal propagating in a 8λ , 512λ coherence length medium, and for a 32λ line array. The processing scheme, which has been used to derive the above array gain estimates has been discussed in Sect. 3.

SACLANTCEN SM-238

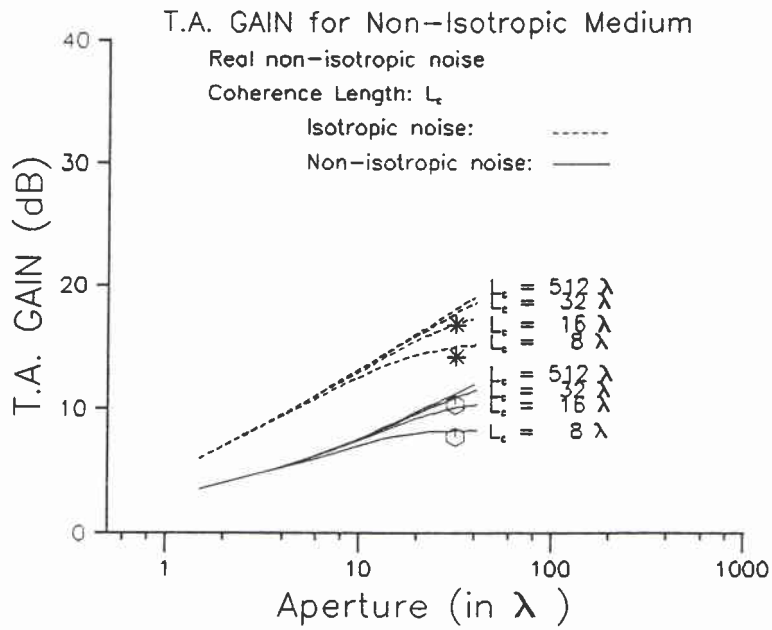


Figure 7 The information in Fig. 6 is for broadside direction of the line array at 30° bearing in the anisotropic noise field shown in Fig. 4. In this figure the same kind of information as in Fig. 6 is derived for broadside direction of the line array at 270° bearing in the above anisotropic noise field.

5

Experiments

Two kinds of experimental setups were used to apply the theoretical development of the present study on real data. The first one included a 64-hydrophone line array towed by a research vessel. Ambient noise measurements obtained with this line array were used to estimate the array gain of a monochromatic signal radiated by a distant ship and to create long synthetic apertures. In the second setup, long towed array measurements from a 256-hydrophone geophysical-type streamer were used to test the validity of the above synthetic aperture results. These long towed array measurements have been provided by the US Office of Naval Research and they originate from experiments carried out by Yen and Carey [25]. The objective in their study was to test a passive synthetic aperture technique that they had developed. Their reported synthetic aperture results are successful and any comparison in performance between the ETAM algorithm and their technique is beyond the scope of the present study.

5.1. 64-HYDROPHONE TOWED ARRAY

The experimental setup included a receiving line array with 64 hydrophones spaced at 1 m. This array was towed at 100-m depth by a vessel moving along a straight-line course at 5 kn. The water depth was 2000 m and aerial surveillance in the area indicated the presence of few ships beyond the 28 km range. The data-acquisition and control system included amplification of the hydrophone signals, bandpass filtering, digitization, and recording on a high-performance digital recorder for off-line processing of the time series. The acoustic field generated by the distant shipping was recorded continuously for a period of 6 min by the towed array while the tow vessel was moving along a straight-line course.

Presented in Fig. 8 is the power spectrum of one of the hydrophone received broadband signals, which has been processed with a numerical bandpass filter centered at 400 Hz. Clearly shown in the above spectrum is the presence in the sampled acoustic field of a monochromatic signal at 400 Hz and of unknown origin. At this frequency, the average signal-to-noise ratio along the sensors of the line array was $\zeta = 21$ dB in the frequency bin. The monochromatic signal embodied in the noise field of the distant shipping has been used in this study to test the theoretical development and the array gain processing scheme, which have been discussed in Sect. 3.

SACLANTCEN SM-238

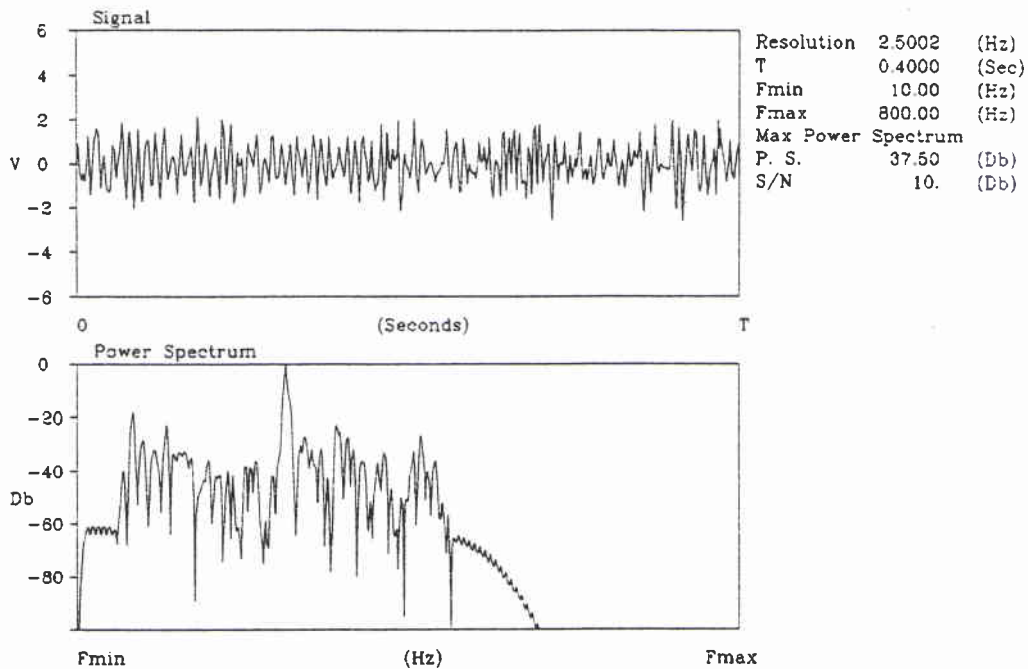


Figure 8 Shown in the upper part is the signal received by the hydrophones of the towed array. The digitized time series have been windowed and filtered to include, in this case, a bandpass frequency regime (250–650 Hz) centred at 400 Hz. In the lower part, the power spectrum of the above decimated time series is shown. The received monochromatic signal at 400 Hz is clearly shown in the above spectrum.

Shown by the solid line in Fig. 9 are the bearing estimates obtained from beamforming at 400 Hz the 512-hydrophone synthetic array derived from the 64-hydrophone physical array using the ETAM algorithm. For comparison, the dotted line in the same figure gives the bearing estimates at 400 Hz from the 64-hydrophone physical array. The averaged azimuthal pattern at 395 Hz of the broadband acoustic field due to distant shipping is given by the dashed line in Fig. 9. Apparently, the above results show a great consistency between the bearing estimates obtained from a long 512-hydrophone synthesized aperture and those derived from the 64-hydrophone physical array. The power levels of the bearing estimates indicate that the 512-hydrophone extended aperture has been synthesized coherently. However, the question that the 512-element aperture has been synthesized in a medium with at least equal coherence length to that of the extended aperture can be addressed by applying our array processing scheme on these measurements.

Figure 10 shows the results of array gain estimates using the above processing scheme for the physical 64-hydrophone array, and for 128, 256 and 512-hydrophone extended apertures. Predictions also of the array gain estimates for 273λ and 17λ medium coherence lengths, and for isotropic and anisotropic noise fields are also shown by the dashed and solid lines, respectively. In order to derive the above array gain predictions and estimates, the power directivity pattern of the anisotropic noise field was considered to be the average azimuthal pattern of the noise field due to

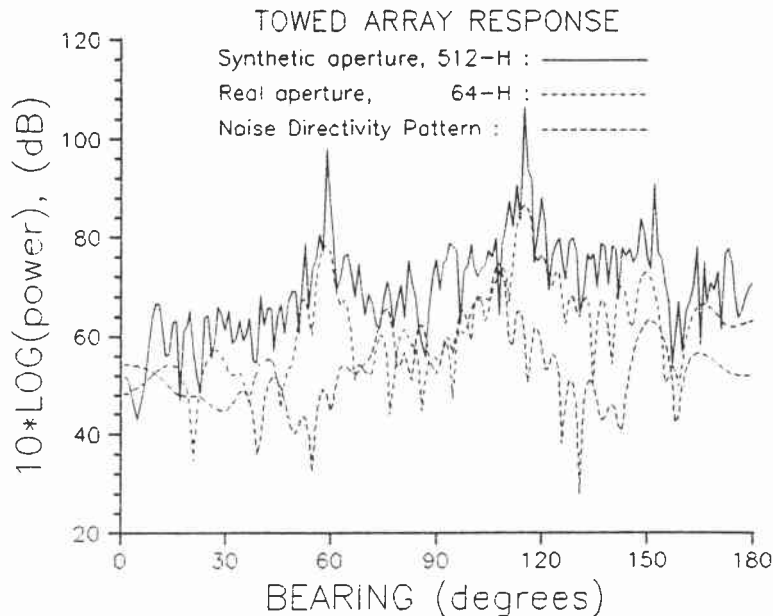


Figure 9 Shown by the solid line are the bearing estimates of the source obtained by beamforming a 512-hydrophone extended towed-array derived from a 64-hydrophone towed-array time series with $T = 175$ s observation period by using the ETAM algorithm. For comparison, the bearing estimates from a 64-hydrophone fully populated array are given by the dotted line. The dashed line shows the average azimuthal power pattern of the noise field due to distant shipping at a frequency regime near 400 Hz that does not include the monochromatic 400 Hz line.

distant shipping, which is shown by the dashed line in Fig. 9. The meaning of the above values of array gain for this kind of anisotropic noise field is related with the array performance to discriminate against distant shipping noise in favour of the desired source signal. Clearly, in Fig. 10 the array gain estimates agree with the predictions for 273λ medium coherence length; this indicates that the coherence properties of the underwater environment in our experimental area are sufficient for long towed array and synthetic aperture applications.

At this point it is considered appropriate to present the broadband frequency dependent directivity pattern of the sampled acoustic field for the above experimental area. Shown at the left-hand side of Fig. 11 is a typical broadband bearing pattern of the above acoustic field for the 250–650 Hz frequency regime obtained from the 64-hydrophone physical aperture; on the right-hand side of this figure is the broadband azimuthal pattern for the 512-hydrophone extended aperture. It is important to note here that the azimuthal power pattern from the extended aperture has all the characteristics of higher angular resolution than those shown by the results of the physical array. An aerial surveillance in the area provided information about the presence of four ships in the azimuthal section of 60–90° at the broadside of the

SACLANTCEN SM-238

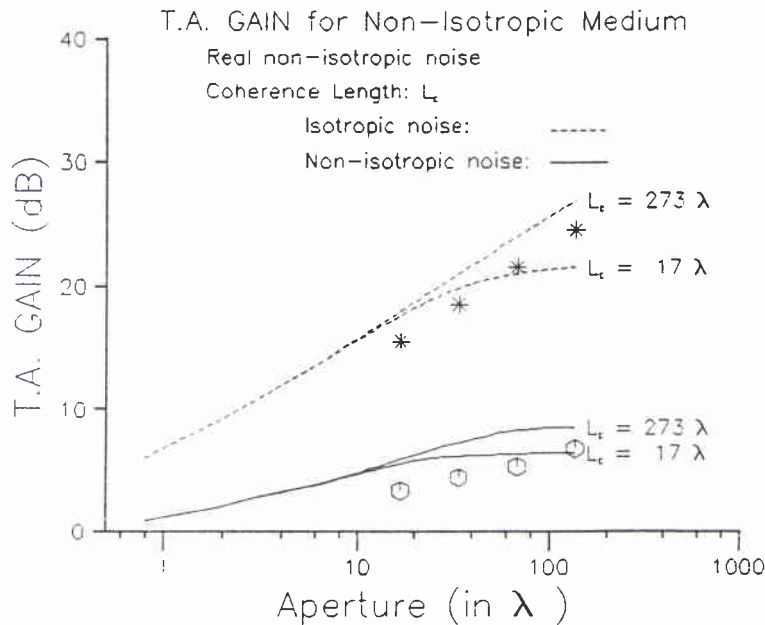


Figure 10 Shown by the solid lines are the array gain estimates for the anisotropic noise field of Fig. 9 due to distant shipping, for different values of spatial coherence length of the medium (i.e. $L_c = (273, 17)\lambda$). The dashed lines give the array gain predictions for isotropic noise field and for the same values of spatial coherence length as before. The data points indicated by a star symbol correspond to array gain estimates for isotropic noise field, for the 400 Hz monochromatic signal, for the 64-hydrophone real array, and for 128, 256, 512-hydrophone extended apertures derived from the 64-hydrophone physical array using the ETAM algorithm. Shown by the hexagon-shaped data points are array gain estimates for the real anisotropic noise field of Fig. 9, for the 400 Hz signal and for the same apertures (i.e. 64, 128, 256, 512-hydrophone) as before. The processing scheme that has been used to derive the above array gain estimates has been discussed in Sect. 3.

towed array. The bearings of these four broadband sources are visible only in the directivity pattern results of the long extended aperture.

From the results of Fig. 11 a speculation can be made about the origin of the monochromatic 400 Hz signal, which was discussed before. The bearing of this signal coincides with that of one broadband source, and it is highly possible that the 400 Hz line is radiated by the above noisy source. The other two bearings (50° and 140°) at 400 Hz are due to reflections from underwater mountains in the area.

Since the sidelobes in Fig. 11 are frequency dependent, a frequency integration of the azimuthal pattern estimates should suppress these sidelobes and give better indications of the bearings related to broadband sources. Presented in Fig. 12 is the integrated power pattern in the frequency regime of 450–650 Hz from the 64-

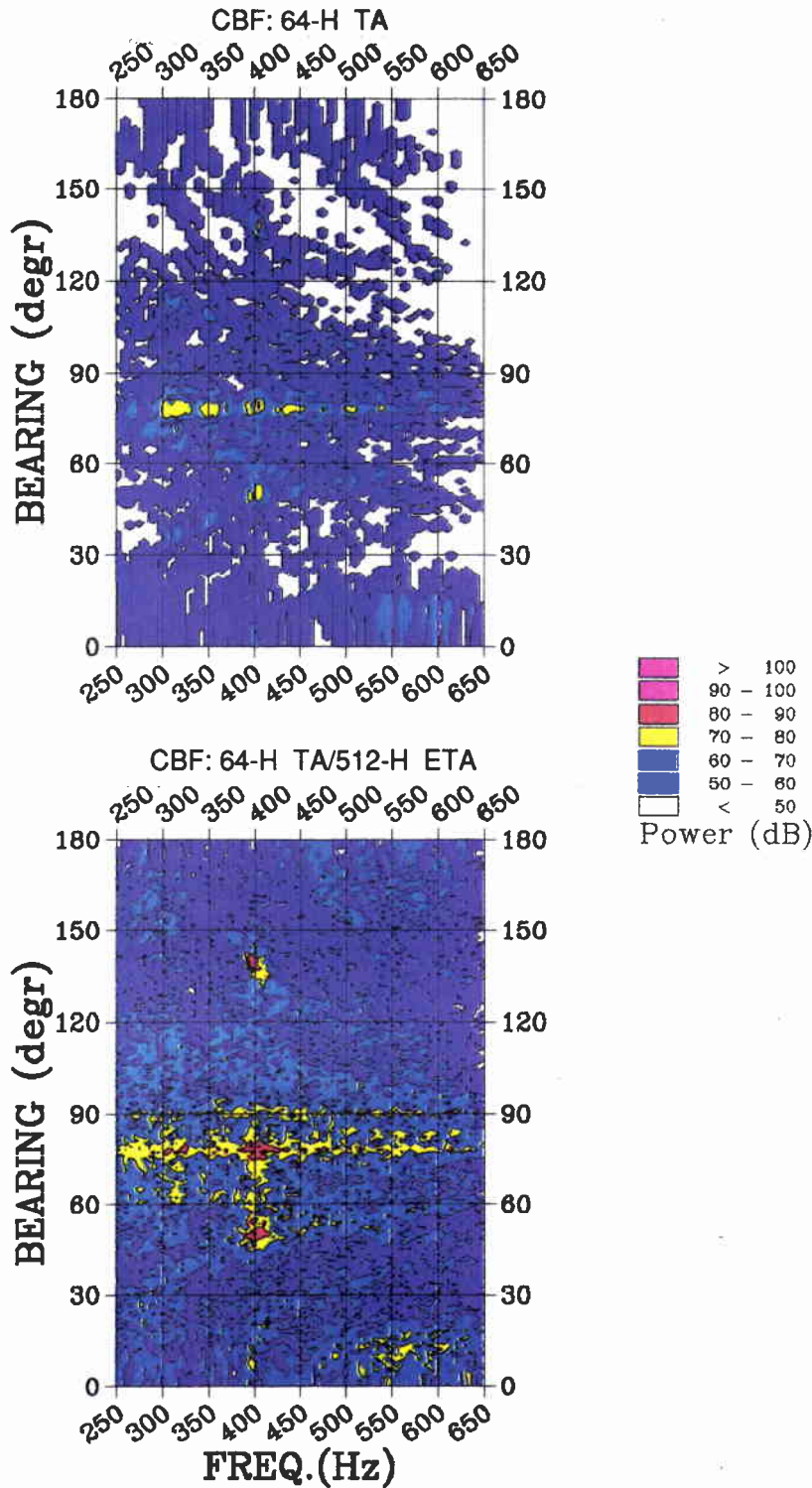


Figure 11 Broadband bearing estimates from a 64-hydrophone physical array and from a 512-hydrophone extended aperture derived from the physical 64-element array using the ETAM algorithm. The frequency regime of these bearing estimates is 250-650 Hz.

 SACLANTCEN SM-238

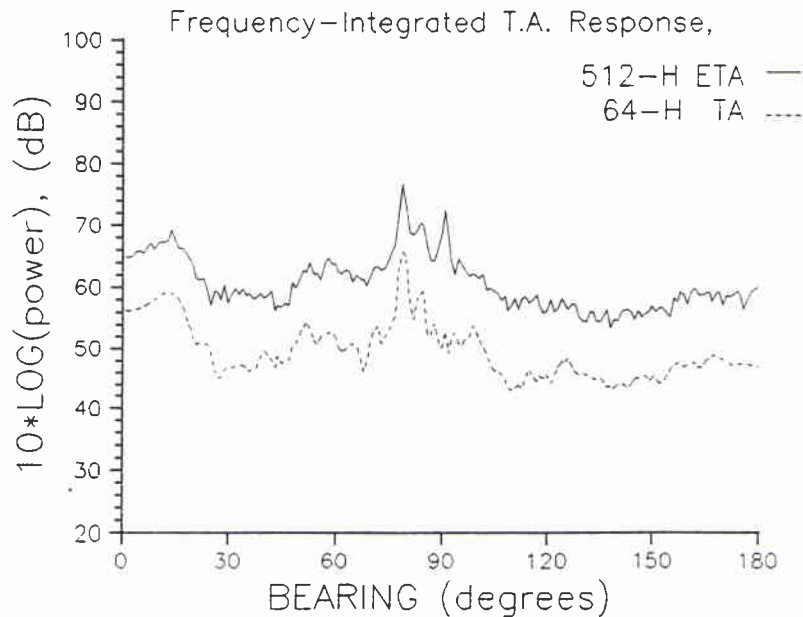


Figure 12 A frequency integrated azimuthal power pattern derived from the results shown in Fig. 11 for the 450-650 Hz frequency regime.

hydrophone physical array and the 512-hydrophone extended aperture. As expected, the results of Fig. 12 are in agreement with those of Fig. 11.

5.2. 256-HYDROPHONE TOWED ARRAY

A geophysical-type streamer, consisting of 256-hydrophones with 2.5-m spacing, was towed at a normal depth of 226 m by a vessel moving along a straight-line course at 2.8 kn and at approximately 200 km from a moored cw source. The water depth was 3200 m and the depth of the source was 300 m. Towed-array data were obtained with a 256-channel digital data acquisition system. These data were Hann windowed and FFT processed in a 0.125 Hz band. Measurements were taken every 13 s and during this period it was expected that the line array had moved by approximately 7.5 hydrophone spacings (i.e. 18.7 m). A detailed description of this experimental setup is given elsewhere [25].

In the present study, the processing method for bearing estimates of the hydrophone array measurements was the conventional beamforming technique without shading, which is an optimum estimator [21]. A typical broadband azimuthal pattern of the acoustic field received by the 256-hydrophone array is shown at the left-hand side of Fig. 13. This pattern is the average from 15 time frames with a time interval of 26 s. In Fig. 13, the presence of a broadband source at 160° bearing and that of the signal at 43° bearing and at 174.5 Hz is very clear. The signal-to-noise ratio was

approximately $c = 3$ dB in the frequency bin, or -8 dB *re* 1-Hz band. The conventional beamforming results at 174.5 Hz of the above towed-array measurements are presented in Fig. 14, which represents a cross section of Fig. 13 at the frequency bin of 174.5 Hz. These results are considered here as a basis for comparison with those from the extended aperture measurements derived from applications of the ETAM algorithm on subapertures of the long-line array.

Presented by the solid line in Fig. 15 are the bearing estimates from beamforming a 256-hydrophone synthesized array at 174.5 Hz, which is derived by the ETAM algorithm from a segment of 32 hydrophones of the actual array. For comparison, the results obtained from beamforming the equivalent physical aperture of the 256-hydrophone array, which are the same with those of Fig. 14, are given by the dashed line. The broadband azimuthal pattern for the above 256-hydrophone synthetic aperture is shown at the right-hand side of Fig. 13, which has the same features as that from the equivalent physical array.

The results in Figs. 16–19 have the same presentation arrangement as those in Figs. 15 and 13, but they refer to longer synthetic apertures. More specifically, Figs. 16 and 17 show bearing results from a 814-hydrophone synthesized aperture derived from an actual 64-hydrophone subarray using the ETAM algorithm, and Figs. 18 and 19 are for a 1024-hydrophone synthesized array derived from a 64-hydrophone physical subaperture. For comparison, the broadband azimuthal pattern derived from the actual 64-hydrophone subarray is shown on the left-hand side of Fig. 17. It is important to note here that the bearing results for the source in the above Figs. 18 and 19 are not so clear as in the previous figures. It is suggested here that this is due to the fact that the upper limit of the spatial coherence length of the medium has been reached, since the results in Figs. 18 and 19 are for a 300λ long synthetic array. This point, however, will be thoroughly examined next, using the theoretical development discussed in Sects. 2 and 3 of this study.

Predictions of the array gain estimates for 300λ and 80λ coherence lengths, and for isotropic and non-isotropic noise fields of the above experimental area, are shown in Fig. 20 by the dashed and solid lines, respectively. In order to derive these array gain predictions, the power directivity pattern of the anisotropic noise was considered to be the frequency-averaged azimuthal pattern of the acoustic field shown in Fig. 13. This averaged pattern is presented in Fig. 21 and it is for a 256-hydrophone actual and synthetic array. In this way, the array gain predictions and estimates for this kind of anisotropic noise are related to the performance of the physical and synthetic array to discriminate the signal against the directive broadband acoustic noise field. The star-shaped data points in Fig. 20 are array gain estimates for 18.4λ , 74.3λ physical apertures and 74.3λ , 150λ , 237λ , 300λ synthetic apertures for isotropic noise field derived according to the processing scheme discussed in Sect. 3. The hexagon-shaped data points are array gain estimates for the same physical and synthetic aperture sizes and for a directive noise field that is shown in Fig. 21. Since the signal-to-noise ratio for these towed-array measurements is below the threshold

SACLANTCEN SM-238

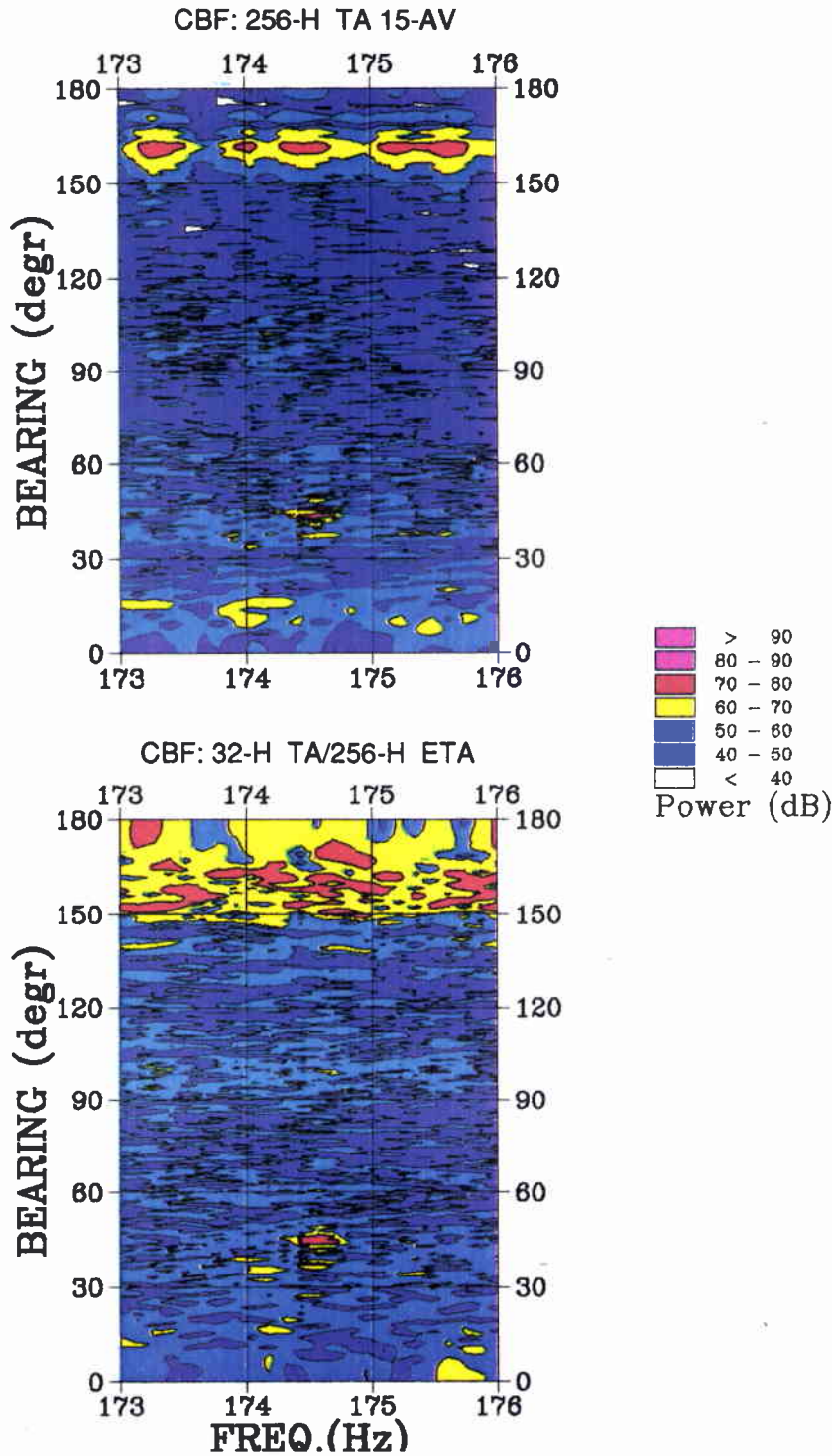


Figure 13 Shown on the left-hand side are broadband bearing estimates from a 256-hydrophone physical array and on the right-hand side from a 256-hydrophone extended aperture derived from a physical 32-element subarray using the ETAM algorithm.

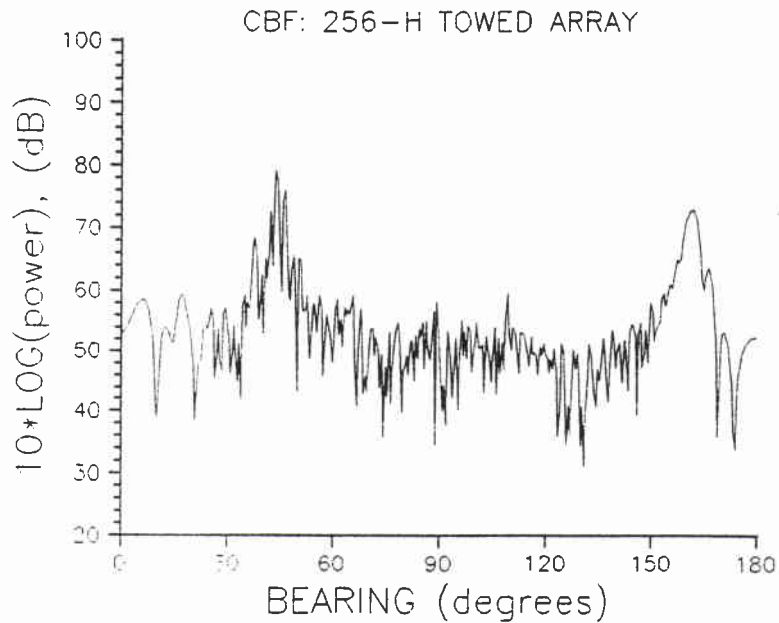


Figure 14 *Bearing estimates of an active at 175 Hz source from real data received by a 256-hydrophone line array with 2.5 m spacing. The range between the projector and the receiver was approximately 200 km, the water depth was 3200 m, and the depth of the receiver and the projector was 220 and 300 m, respectively.*

value of 5 dB of the array gain processing scheme, the above array gain estimates are probably smaller than the predictions by 3–4 dB, which is a very high difference as compared with that of the simulations and the real data presented in Sect. 4 and Subject. 5.1.

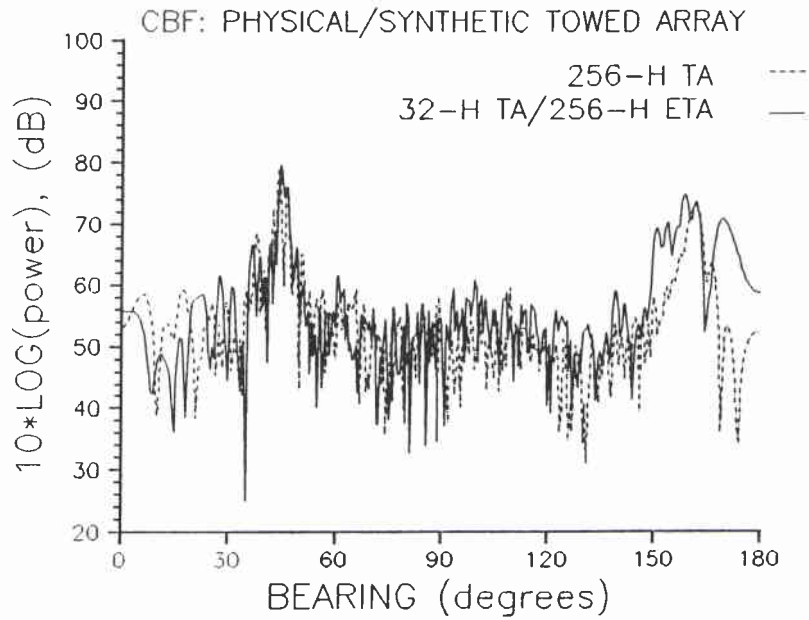
SACLANTCEN SM-238

Figure 15 Shown by the solid line are the bearing estimates of the same source as in Fig. 14 from 256-hydrophone extended-towed-array measurements derived from a 32-hydrophone physical subarray using the ETAM algorithm. For comparison, the bearing estimates from the equivalent fully populated physical array are given by the dashed line, which has the same results as those in Fig. 14.

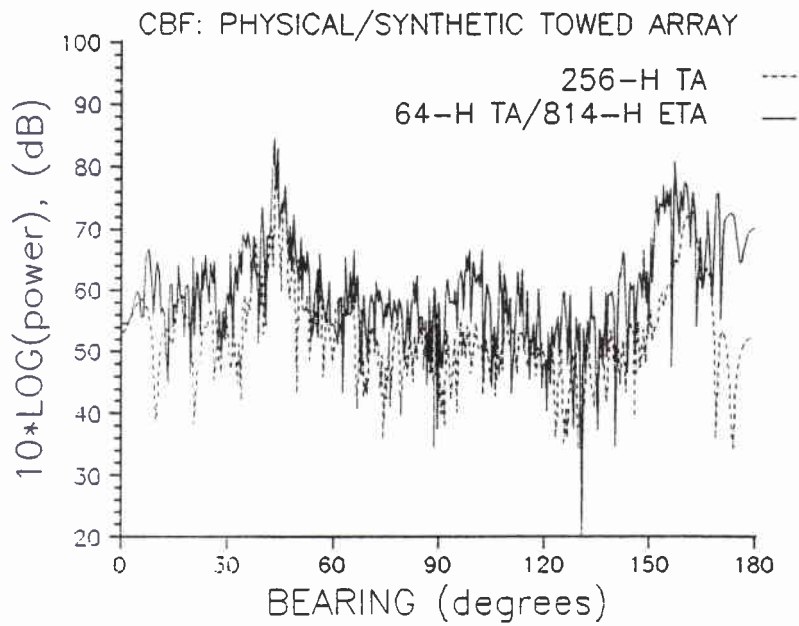


Figure 16 *Bearing estimates of the source from 814-hydrophone extended-towed-array measurements derived from a 64-hydrophone physical subarray using the ETAM algorithm. For comparison, the bearing estimates from the 256-hydrophone physical array are given by the dashed line, which has the same results as those in Fig. 14.*

SACLANTCEN SM-238

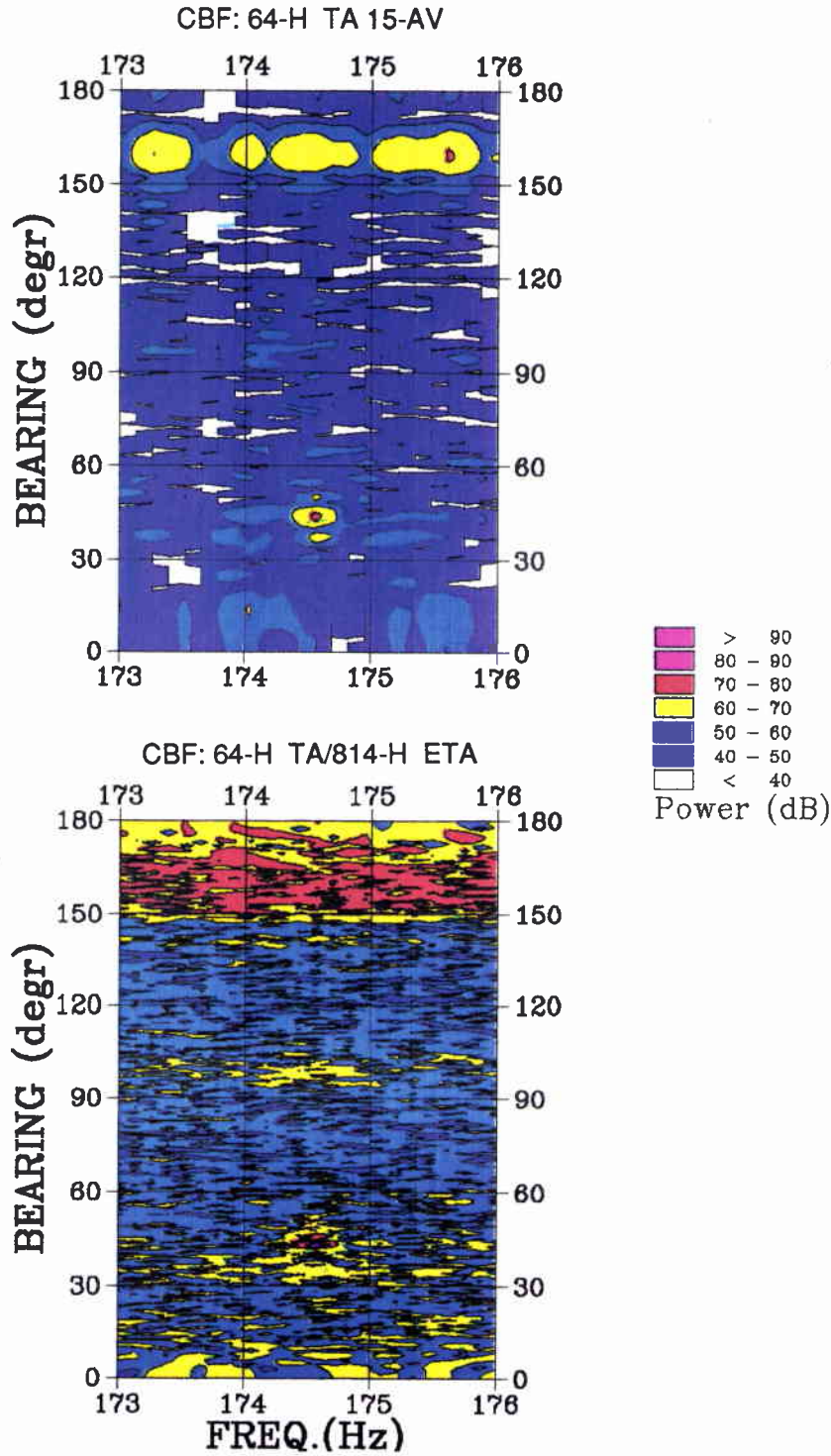


Figure 17 Shown on the left-hand side are broadband bearing estimates from a 64-hydrophone physical subarray and on the right hand side from a 814-hydrophone extended aperture derived from the physical 64-element subarray using the ETAM algorithm.

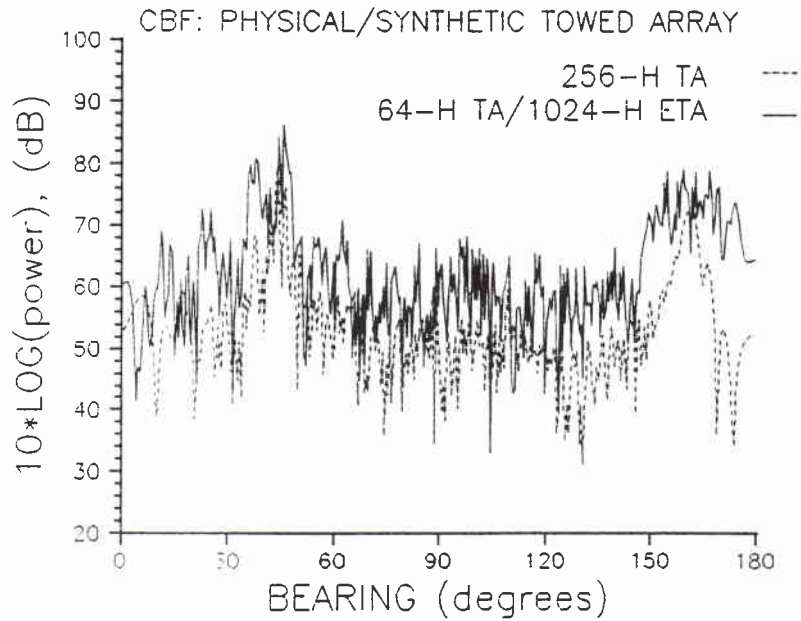


Figure 18 Bearing estimates of the cw source from 1024-hydrophone extended-towed-array measurements derived from a 64-hydrophone physical subarray using the ETAM algorithm. For comparison, the bearing estimates from the 256-hydrophone physical array are given by the dashed line. The arrangement of this set of results is the same as in Figs. 14-16.

SACLANTCEN SM-238

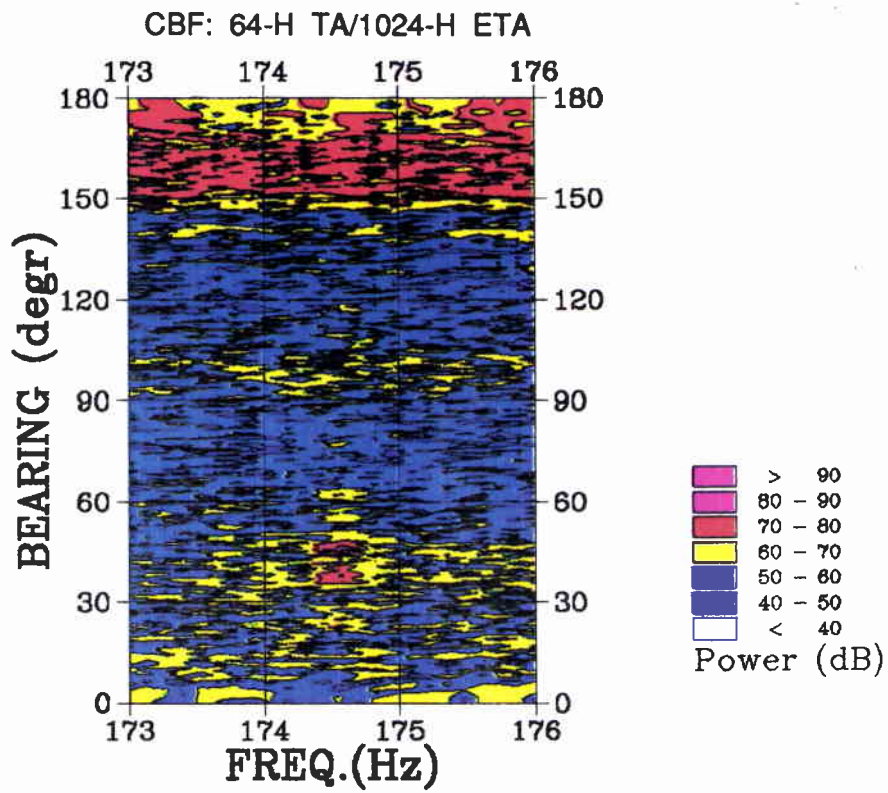


Figure 19 *Broadband bearing estimates from a 1024-hydrophone extended aperture derived from a physical 64-element subarray using the ETAM algorithm. The frequency regime of these bearing estimates is 173-176 Hz.*

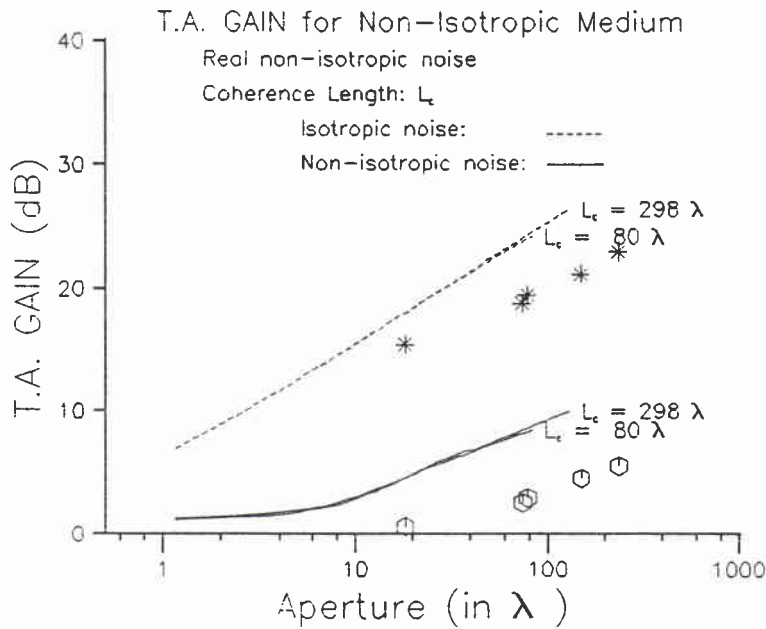


Figure 20 Shown by the solid lines are the array gain predictions for the anisotropic noise field of Fig. 21 due to distant shipping, for different values of spatial coherence length of the medium (i.e. $L_c = (300, 80)\lambda$). The dashed lines give the array gain predictions for isotropic noise field and for the same values of spatial coherence length as before. The data points indicated by a star symbol correspond to array gain estimates for isotropic noise field, for the 175 Hz signal, for a 64-hydrophone and 256-hydrophone real array, and for 256, 512, 814, 1024-hydrophone extended apertures derived from a 32, 64-hydrophone physical subarray using the ETAM algorithm. Shown by the hexagon-shaped data points are array gain estimates for the real anisotropic noise field of Fig. 21, for the 175 Hz signal and for the same apertures as before. The processing scheme that has been used to derive the above array gain estimates has been discussed in Sect. 3.

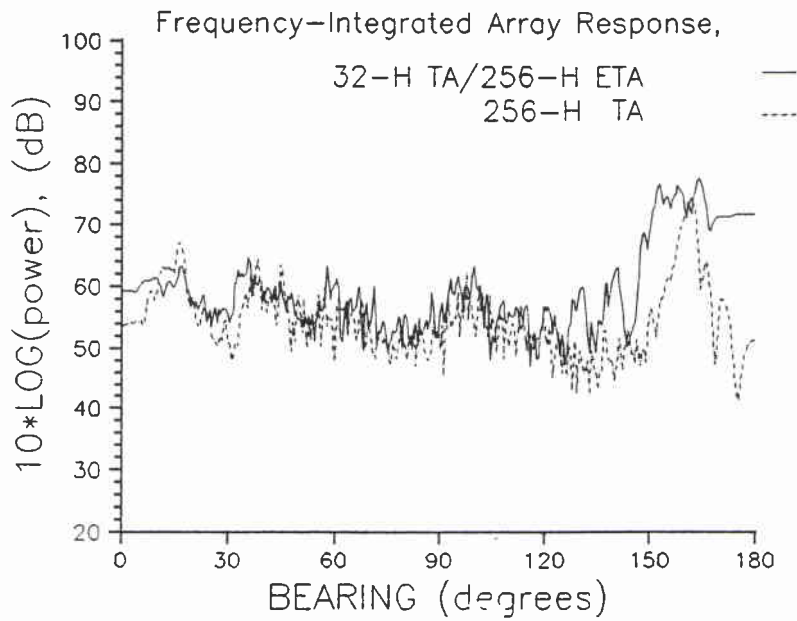
SACLANTCEN SM-238

Figure 21 A frequency-integrated azimuthal power pattern derived from the results shown in Fig. 13 for the 173-174.5 Hz frequency regime for a physical and synthetic aperture. This azimuthal pattern has been considered as an ambient anisotropic noise field for the derivation of the array gain estimates and predictions shown in Fig. 20.

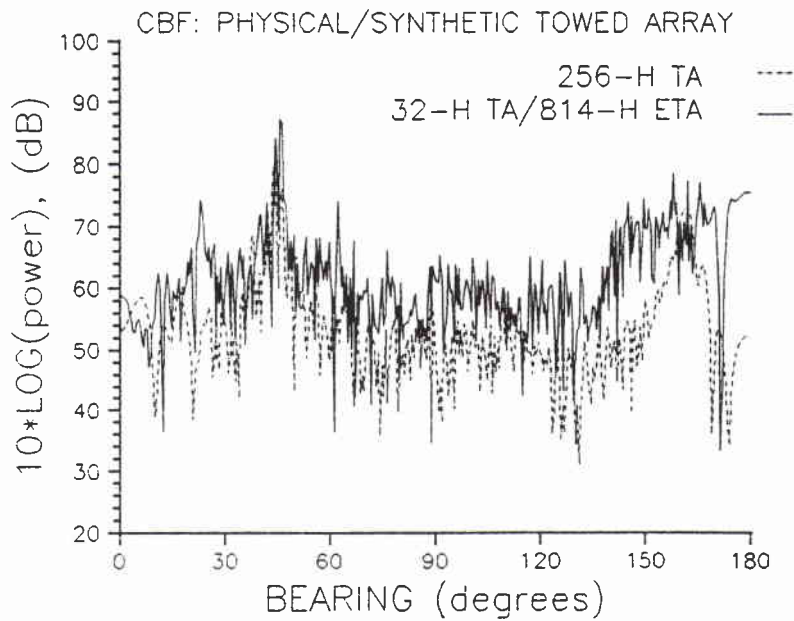


Figure 22 Shown by the solid line are the bearing estimates of the same source as in Fig. 14 from 814-hydrophone extended-towed-array measurements derived from a 32-hydrophone physical subarray using the ETAM algorithm. For comparison, the bearing estimates from the 256-hydrophone physical array are given by the dashed line, which has the same results with those in Fig. 14.

6

Conclusions

The theoretical development for array gain estimates derived from the directivity power pattern of the received signal by assuming that the power pattern of the noise field is known, has been tested with synthetic and real data. Array gain estimates using this method are in agreement with predictions when the signal-to-noise ratio of the received signal is higher than 5 dB in the frequency bin, which is an empirical threshold value derived from simulations.

A comparison of experimental estimates of towed-array gains with gain predictions derived according to Eq. (16) can provide approximate estimates of the spatial coherence length of the medium when the signal-to-noise ratio of the received signal exceeds the threshold value of 5 dB, and the signal and the noise are uncorrelated. When the agreement between the experimental array gain estimates and the predictions is not very good due to very poor signal-to-noise ratio, then the approximate estimates of the spatial coherence length of the medium can be derived from the array gain estimates directly. In other words, the experimental array gain estimates will linearly increase up to an aperture size that is equivalent to the spatial coherence length of the medium, and all the other gain estimates for longer apertures will asymptotically reach a constant array gain value. This case is demonstrated by the results of Fig. 20, where the agreement between the array gain estimates and predictions is very poor due to the small value of signal-to-noise ratio ($\zeta = -8$ dB *re* 1-Hz band). These results indicate that the linear increase in array gain estimates is for values of array aperture smaller than 200λ , which is probably the spatial coherence length of the medium.

A question that is needed to be addressed here is related to the accuracy of the estimates of the spatial coherence length of the medium derived from the inversion method by comparing experimental array gain estimates with gain predictions according to Eq. (16). One way to address this question is to consider the following arguments:

1. The expected spatial coherence length of an underwater area is considered to be of the order $0(10^2)\lambda$. Therefore, this inversion method has practical importance for long towed array or synthetic aperture, i.e. $0(10^2)\lambda$ applications.
2. The array gain processing technique provides experimental gain estimates that are smaller than their expected values by 1 dB when the signal-to-noise ratio of the received signal is in the range of 5–10 dB.

For higher values of ζ this difference is reduced significantly. However, the biased gain estimates by 1 dB will be in agreement with gain predictions that correspond to a medium with smaller spatial coherence length than its expected value by $0(10^1)\lambda$. In other words, from a single experimental gain estimate the inversion method will provide biased estimates of the coherence length of an underwater area. These biased estimates are smaller than their expected values by 10–20%. One way to improve the accuracy of the estimates of the coherence length of the medium is to derive them directly from the experimental array gain estimates in the same way as in the case of a very poor signal-to-noise ratio discussed before.

Real data applications have indicated that the coherence properties of the ocean can be sufficient for effective long towed-array operations and the extension of the physical aperture of a conventional towed array by more than one order of magnitude can be successful. The results presented (Figs. 13–15) have shown that the broadside bearing estimates from a 256-hydrophone synthetic aperture derived from a 32-hydrophone subarray are nearly identical with those from an equivalent 256-hydrophone fully populated physical array. Also, the formation of very long synthesized apertures, as in the case of an 814-hydrophone extended aperture derived from a 64-hydrophone subarray (Figs. 16 and 17), includes all the expected features of improved angular resolution. If this long synthetic aperture had been derived from a smaller 32-hydrophone subaperture using the ETAM algorithm, the results would have been nearly identical according to the predicted performance of the above technique [21]. This is demonstrated by the results of Fig. 22 where the power azimuthal pattern from an 814-hydrophone synthetic array derived from a 32-hydrophone subarray is shown and these results are comparable with those in Fig. 16.

At this point, it is important to discuss the bearing results for the broadband source at the endfire of the towed array shown in Figs. 15–22. It has been demonstrated that for the case of broadband signals the performance of the ETAM algorithm is successful [24] and this is shown by the results in Fig. 11. The endfire broadband bearing estimates in Figs. 15–22 from the extended aperture measurements, however, suggest that the ETAM algorithm in this case does not provide sharply defined bearing results. The cause of this failure may be due to the array deformation at the endfire or to an artifact created by the algorithm itself. Future experiments, including ships as broadband sources and signals, have been planned to clarify this ambiguity.

References

- [1] Wille, P. and Thiele, R. Transverse horizontal coherence of explosive signals in shallow water. *Journal of the Acoustical Society of America*, **50**, 1971: 348–353.
- [2] Clay, C.S. and Medwin, H. High-frequency acoustical reverberation from a rough-sea surface. *Journal of the Acoustical Society of America*, **36**, 1964: 2131–2134.
- [3] Schulkin, M. and Shaffer, R. Backscattering of sound from the sea surface. *Journal of the Acoustical Society of America*, **36**, 1964: 1699–1703.
- [4] Marsh, H.W. Sound reflection and scattering from the sea surface. *Journal of the Acoustical Society of America*, **35**, 1963: 240–244.
- [5] Middleton, D. Acoustic scattering from composite wind-wave surfaces in ‘bubble-free’ regimes. *IEEE Journal of Oceanic Engineering*, **14**, 1989: 17–75.
- [6] Kuperman, W.A. and Ingenito, F. Attenuation of the coherent component of sound propagating in shallow water with rough boundaries. *Journal of the Acoustical Society of America*, **61**, 1977: 1178–1187.
- [7] Berman, D.H. and McCoy, J.J. Coherence propagation and geometric acoustics. *Journal of the Acoustical Society of America*, **79**, 1986: 635–643.
- [8] Frankenthal, S. The mutual coherence function in a scattering channel: a two-scale solution. *Journal of the Acoustical Society of America*, **85**, 1989: 104–113.
- [9] Dozier, L.B. Spatial coherence in shallow water. NRL SAIC-85/1035. Washington D.C., Naval Research Laboratory, 1985.
- [10] Uscinski, B.J. Acoustic scattering by ocean irregularities: aspects of the inverse problem. *Journal of the Acoustical Society of America*, **79**, 1986: 347–355.
- [11] Uscinski, B.J., Potter, J.R. and Akal, T. Broad-band acoustic transmission fluctuations during NAPOLI 85, an experiment in the Tyrrhenian Sea: Preliminary results and an arrival-time analysis. *Journal of the Acoustical Society of America*, **86**, 1989: 706–715.
- [12] McDaniel, S.T. Vertical spatial coherence of scattering from the Arctic ice canopy: Comparison of theory with experiment. *Journal of the Acoustical Society of America*, **85**, 1989: 2378–2382.
- [13] McDaniel, S.T. Physical optics theory of scattering from the ice canopy. *Journal of the Acoustical Society of America*, **82**, 1987: 2060–2067.
- [14] Adams, S.L. and Doubek, J.W. Frequency coherence and time coherence in random multipath channels. *Journal of the Acoustical Society of America*, **62**, 1977: 286–294.
- [15] Beran, M.J., McCoy, J.J. and Adams, B.B. Effects of a fluctuating temperature field on the spatial coherence of acoustic signals, NRL 7809. Washington D.C., Naval Research Laboratory, 1975.
- [16] Fitzgerald, R.M., Guthrie, A.N. and Shaffer, J.D. Transverse coherence of low frequency signals, NRL 8241. Washington D.C., Naval Research Laboratory, 1978.
- [17] Yen, N. Ambient-sea-noise directionality: Measurement and processing. *Journal of the Acoustical Society of America*, **62**, 1977: 1176–1188.

- [18] Wasiljeff, A. Spatial horizontal coherence of acoustical signals in shallow water, SACLANTCEN SM-68. La Spezia, Italy, NATO SACLANT Undersea Research Centre, 1975. [AD A 011 560]
- [19] Bello, P.A. Characterization of randomly time-variant linear channels. *IEEE Transactions on Communications Systems*, **10**, 1963: 360-393.
- [20] Autrey, S.W. Passive synthetic arrays. *Journal of the Acoustical Society of America*, **84**, 1988: 592-598.
- [21] Stergiopoulos, S. and Sullivan, E.J. Extended towed array processing by an overlap correlator. *Journal of the Acoustical Society of America*, **86**, 1989: 158-171.
- [22] Nuttall, A.H. and Carter, G.C. Approximations for statistics of coherence estimators, NUSC TR 5291. New London, CT, Naval Underwater Systems Center, 1976.
- [23] Mohnkern, G.L. Maximum likelihood estimation of magnitude-squared coherence, NOSC TR 717. San Diego, CA, Naval Ocean Systems Center, 1981.
- [24] Stergiopoulos, S. Optimum bearing resolution for a moving towed array and extension of its physical aperture, SACLANTCEN SR-154. La Spezia, Italy, NATO SACLANT Undersea Research Centre, 1989. [AD B 136 086]
- [25] Yen, N. and Carey, W. Application of synthetic-aperture processing to towed-array data. *Journal of the Acoustical Society of America*, **86**, 1989: 754-765.
- [26] Carey, W.M. and Moseley, W.B. Space-time processing, environmental-acoustic effects. In: Merklinger, H.M., ed. *Progress in Underwater Acoustics*. New York, NY, Plenum, 1987: 743-758.
- [27] Flatté, S.M., Dashen, R., Munk, W.H., Watson, K.M., Zachariasen, F. *Sound Transmission through a stratified fluctuating ocean*. Cambridge, UK, Cambridge University Press, 1979.
- [28] Flatté, S.M. Wave propagation through random media: Contributions from ocean acoustics. *Proceedings of the IEEE*, **71**, 1983: 1267-1294.
- [29] Beran, M.J. and McCoy, J.J. Propagation through an anisotropic random medium. *Journal of Mathematical Physics*, **15**, 1974: 1901-1912. Propagation of radiation from a finite beam or source through an anisotropic random medium. *Journal of the Acoustical Society of America*, **56**, 1974: 1667-1672.
- [30] Urick, R.J. *Principles of Underwater Sound for Engineers*. New York, NY, McGraw-Hill, 1967: p. 49.
- [31] Shifrin, Y.S. *Statistical Antenna Theory*. Boulder, CO, Golem Press, 1971: p. 40.
- [32] Cron, B.F. and Sherman, C.H. Spatial correlation functions for various models. *Journal of the Acoustical Society of America*, **34**, 1962: 1732-1736.
- [33] Wagstaff, R.A. Iterative technique for ambient-noise horizontal-directionality estimation from towed line-array data. *Journal of the Acoustical Society of America*, **63**, 1978: 863-869.

Initial Distribution for SM-238

SCNR for SACLANTCEN

SCNR Belgium	1
SCNR Canada	1
SCNR Denmark	1
SCNR Germany	1
SCNR Greece	1
SCNR Italy	1
SCNR Netherlands	1
SCNR Norway	1
SCNR Portugal	1
SCNR Spain	1
SCNR Turkey	1
SCNR UK	1
SCNR US	2
SECGEN Rep. SCNR	1
NAMILCOM Rep. SCNR	1

National Liaison Officers

NLO Canada	1
NLO Denmark	1
NLO Germany	1
NLO Italy	1
NLO Netherlands	1
NLO UK	1
NLO US	4
Total external distribution	26
SACLANTCEN Library	10
Stock	24
Total number of copies	60